Chapter 2
Nanostructures for Enhanced Light-Trapping in Thin-Film Silicon Solar Cells

2.1 Introduction

The demand for low-cost, high-efficiency solar cells along with the never-ending promises of modern technology have caused an increase of research into photovoltaics, particularly into the control of light at the subwavelength scale. In fact, the now well known Shockley and Queisser paper about the limiting efficiency of solar cells [1] was a "sleeping beauty" for almost 40 years of slow reception [2].

Accordingly, a multiplicity of light-trapping concepts has been proposed with the intent of enhancing the optical depth of thin-film absorbers; the more light-trapping approaches are developed, the more marketable options will be explored, with the more promising ones having an impact on thin-film solar cells: nanophotonis therefore drives the vision of a new generation of photovoltaic devices.

Before I focus on the diffractive designs I pursued in my project, I will first give a brief overview of the main techniques in Sect. 2.2. I then analyse the model of an ideal scattering structure in Sect. 2.3, called Lambertian texture, which led me to introduce a figure-of-merit in Sect. 2.4, called the light-trapping efficiency (*LTE*), that can purely assess the performance of a light-trapping technique itself – irrespective of the material, fabrication method and technology used. Before I apply the *LTE* to state-of-the-art proposals to identify the most promising strategies, I will review the important milestones of light-trapping for photovoltaics in Sect. 2.5 and finally conclude with some specific remarks regarding future trends in Sect. 2.6.

2.2 The Main Light-Trapping Approaches

2.2.1 Non-diffractive Techniques

Maximizing the surface-to-volume ratio is the most intuitive way of enhancing the probability of photon absorption. Silicon **nanowires** are examples for such light-

C.S. Schuster, *Diffractive Optics for Thin-Film Silicon Solar Cells*,
Springer Theses, DOI 10.1007/978-3-319-44278-5_2

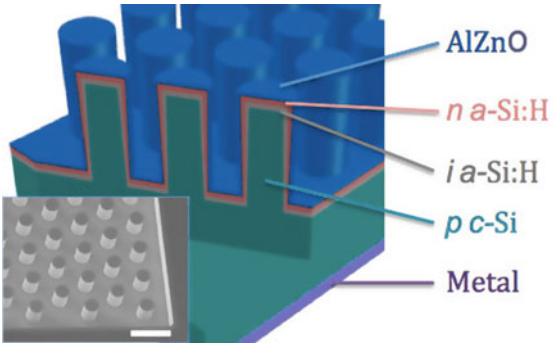

Fig. 2.1 Schematic of a Heterojunction with Intrinsic Thin Layer (HIT) radial junction silicon solar cell with 10 % power conversion efficiency [4]. A 30° tilted *top-view* image of a fabricated device is shown in the inset. The indicated scale bar as well as the pillar's length are 10 μm

trapping strategies, where the electronic transport properties may additionally benefit from a radial junction, as illustrated in Fig. 2.1. Solar cell devices with conversion efficiencies of around 12 % were reported for a nanowire junction geometry [5, 6] whereas the use of nanowires as an anti-reflection texture for 300 μm thick substrates enabled device efficiencies of 18 % [3, 7].

However, too many research challenges still need to be addressed, before a commercial product based on nanowires can be introduced: mainly, the stability of the junction formation and the effective surface passivation, but also practical issues, such as the rapid scaling and the integration of nanowires into modules, need to be better understood and further improved.

Another method for enhancing the photon absorption takes advantage of the **plasmonic resonance** of metal nanoparticles. Metal nanoparticles can exhibit a very high polarizability at the resonance wavelength, and efficiently scatter the incident light into the thin-film. Here, the particle dimensions are a key parameter for the tuning of the resonance condition.

Solar cells with plasmonic scatterers have attracted a lot of attention [8], but the proposed effect turned out to be very sensitive to the material parameters. While enhancements of up to 30 % in the power conversion efficiency were reported for plasmonic thin-film silicon solar cells, the absolute power conversion efficiency remained below 10 % [9–13].

One of the issues I study later (see Sect. 4.3) is the dissipative loss of such plasmonic structures; therefore, if the plasmonic scatterers were replaced by dielectric structures, the dissipative optical losses could be greatly reduced.

In fact, dielectric **Mie resonators** were recently proposed by Spinelli et al. [14]. The authors could demonstrate almost perfect impedance matching from the ultraviolet to the near-infrared spectral range using Si nanopillar arrays, i.e. less than 3 % reflectivity was obtained over the entire spectral range 450–900 nm by 150 nm long nanowires with a 0.5 μm array pitch and 60 nm thick Si_3N_4 overlay coating.

To characterize the wavelength dependent scattering efficiency Q_{sca}, the scattering cross section σ_{sca} is usually normalized to the geometrical area of the structure σ_{geom}. For dielectric Mie resonators, scattering efficiencies $Q_{sca} = \sigma_{sca}/\sigma_{geom}$ up to 10 have been demonstrated so far [14].

In addition, it has also been demonstrated that Mie-resonators could even be placed on top of an already completely finished thin-film solar cell for enhancing its power conversion efficiency [15].

Thin and transparent dielectric coatings are a further and well-known anti-reflective technique. Commonly used materials are SiO_x, Si_3N_4, and some conductive oxides like SnO_2, ZnO or tin-doped indium oxide (ITO) to name but a few [18]. Since the Fresnel-reflection

$$R = \left(\frac{n_1 - n_2}{n_1 + n_2}\right)^2 \tag{2.1}$$

strongly depends on the refractive index contrast of two bordering media with refractive indices n_1 an n_2, an intermediate 'buffer' layer can be used to reduce the reflection. For example, if a coating with refractive index $n_{AR} = \sqrt{n_1 \cdot n_2}$ is chosen a quarter wavelength thick $\lambda/4n_{AR}$, the incident and reflected waves will largely cancel each other out by destructive interference. Anti-reflective coatings can thus be understood as optical-impedance matching layers at the interface between two bordering materials, e.g. air/semiconductor.

Ideally, the refractive index would vary continuously in the transition region from air to silicon, because one single coating can not meet the requirement for a broadband anti-reflective quality. Such an inhomogeneous refractive index profile is approximated by multiple coatings, increasing the refractive index stepwise. A triple layer system of $ZnS/MgF_2/SiO_2$, for example, has shown to reduce the silicon reflectance down to 2 % in the wavelength range from 440 to 960 nm [19].

However, the fabrication of such multilayer coatings is often too expensive for most commercial solar cells. In addition, the anti-reflection effect is very sensitive to the layer's thickness as well as to the angle of the incident light. For oblique incident light, the performance of thin film coatings can indeed dramatically change.

2.2.2 Refractive Approaches

A varying refractive index at the interface of two bordering materials may be mimicked by a surface texture. The eye of a moth, for example, is inherently covered with sub-wavelength cone-shaped structures, helping moths to evade detection by predators and maximizing light capture for vision.

For wavelengths much larger than the typical feature sizes, the effect can be understood by a breakdown of the texture into multiple layers; the aspect-ratio thereby corresponds to the transition region from air to silicon. Approximately, and in analogy to anti-reflection multi-layer coatings, such textures can be described as a medium with an effective index stepwise increasing from air to silicon, as illustrated in Fig. 2.2a.

On the other hand, textures with dimensions of a few tens of micrometer can also reduce the external reflection of sunlight. If the wavelengths are much smaller than the structural feature sizes, radiation will generally bounce onto the textured surface multiple times (rather than out to the surrounding air), as illustrated in Fig. 2.2b.

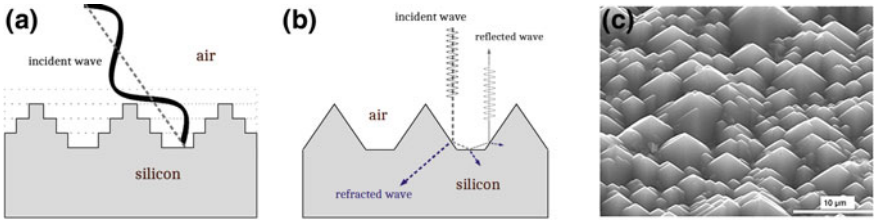

Fig. 2.2 **a** If the typical feature sizes are smaller than the incident wavelength, light will see the texture as an inhomogeneous medium with an effective refractive index gradually increasing from air to silicon. In analogy to a multi-layer anti-reflection coating, this effect reduces the reflection dramatically. **b** If the typical feature sizes are larger than the incident wavelength, light will usually undergo multiple reflections on the textured surface, which in turn increases its probability of entering the absorber material. Since light is also refracted at the air-silicon interface, the path length through the absorber slab will be longer compared to the flat surface situation. **c** Large square-based random pyramids often form the surface of an appropriately textured crystalline silicon solar cell [21], exploiting both anti-reflective and refractive effects in order to enhance sunlight absorption

In addition, light changes its propagation direction when entering a different material, since the speed of light depends on the medium. The effect is called **refraction** (from the Latin word 'refringere') following the fact that an object partly in one medium and partly in another medium appears to be broken, e.g. a stick that is partly submersed in the water.

Refraction at surface textures therefore appears as a natural choice for enhancing the properties of a solar cell, because it affords the redirection of sunlight into the absorber layer without incurring additional losses. The surface of most commercial crystalline silicon solar cells are indeed textured with anti-reflective/refractive pyramids similar to those shown in Fig. 2.2c.

In conclusion, refractive textures in combination with sub-wavelength features (as those shown in Fig. 2.3) may enable efficient light-trapping action over a broad spectral and angular range.

On the basis of this idea, Han et al. recently outlined an economical way for suppressing the surface reflection of a polished silicon wafer from 30 to 3 % between 400 and 900 nm wavelength [21], as illustrated in Fig. 2.3.

2.2.3 Diffractive Approaches

Light is redirected when it bounces off a barrier (reflection) or goes from one medium to another (refraction). However, light may also change its propagation direction as it passes through an opening or around an obstacle in its path. Since the incident light thereby breaks up into different directions, the phenomenon is called diffraction (from the Latin word 'diffringere'). Consequently, light can be diffracted at a surface texture, if its ridges and growths are understood as the openings and obstacles.

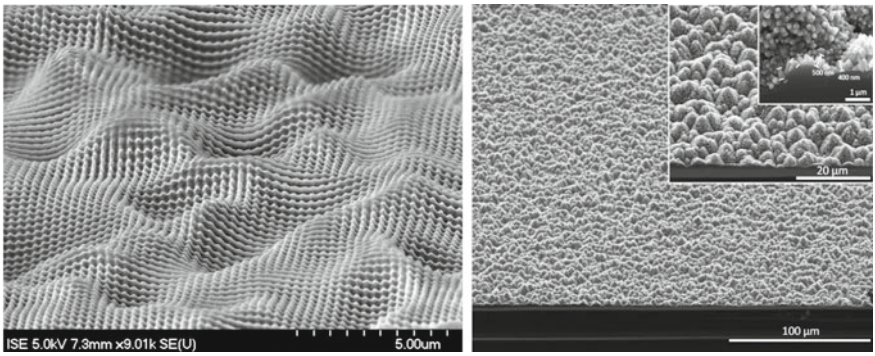

Fig. 2.3 A periodic refractive microstructures in combination with moth-eye sub-wavelength textures can provide excellent anti-reflection properties according to B. Bläsi [22] (*left image*) and S. Han et al. [21] (*right image*)

Augustin-Jean Fresnel [23] was first able to explain diffraction as the resulting interference pattern of waves that were formed behind openings or obstacles. The superposition of all diffracted waves is commonly known as the diffraction pattern; mathematically, it is derived from a Fourier-transform of the diffracting structure.

In order to exploit diffractive effects, the typical structural sizes Λ need to be similar to the incident wavelength λ as illustrated in Fig. 2.4.

For example, radiowaves can bend around mountains in contrast to microwave (mobile phone) signals. Bat's echo calls are rather reflected than diffracted from their

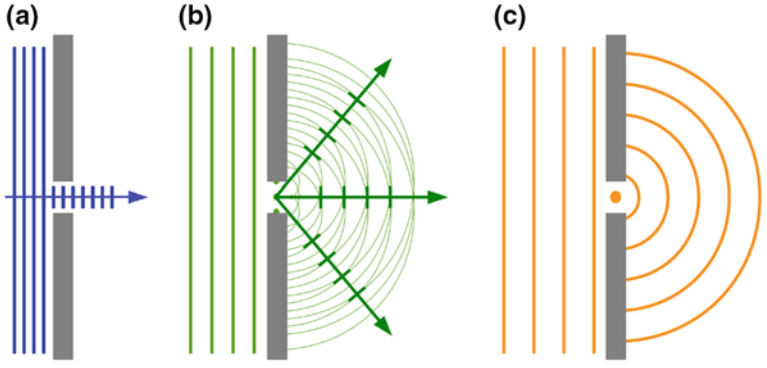

Fig. 2.4 The drawings illustrate three possible interactions for wavefronts of light – coming from a distant source – with the opening of a barrier. **a** If the wavelength is much smaller than the slit width, light propagation can be approximated by geometrical ray optics. **b** If the wavelength is of similar size than the slit width, light will interfere and form a diffraction pattern behind the slit. The wavefronts of the constructive interfering waves are indicated as small bars. **c** If the wavelength is much larger than the slit width, the slit is considered as a source of a new propagating wave behind the slit

prey ($\lambda \ll \Lambda$), whereas an object would be impossible to resolve when it is smaller than the wavelength with which it is observed ($\lambda \gg \Lambda$).

If the degree of diffraction depends on the relationship between λ and Λ, white sunlight can split into its colours when it interacts with a diffractive structure.

Ideally, a diffractive structure on the surface of a silicon solar cell would deflect the longer wavelengths into the plane of the silicon absorber, because those wavelenghts require absorption lengths often beyond the absorber thickness.

If the silicon slab is further embedded in a low-index material, like air, diffracted light may also be totally internally reflected back at the cladding. In this case, light is trapped in the plane of the silicon absorber layer – the key goal that light trapping tries to achieve. A thin-film silicon solar cell with a light-trapping nanostructure then behaves similarly to a waveguide and the nanostructure can be understood as the coupling interface for sunlight.

2.2.3.1 The Grating Equation

Since diffraction results in a change in direction, the incident photon needs to exchange momentum with the grating. The energy and momentum of the incident photon must thereby be conserved, while – in analogy to the crystal lattice momentum in a solid– the transfer of a grating momentum G is restricted to integer multiples m of G, which is directed parallel to the grating's surface:

$$k \cdot \sin\theta_{in} + m \cdot G = k \cdot \sin\theta_m \qquad \text{with } G = \frac{2\pi}{a} \tag{2.2}$$

Here, a is the spatial period of the grating structure and θ_{in} and θ_m are the incident angle and diffraction angle of the mth-order, respectively, as illustrated in Fig. 2.5. The angles are defined as positive when measured counter-clockwise.

If λ stands for the free-space wavelength of light, $k = 2\pi/\lambda$ for the wave-number and n_1 and n_2 are the wavelength dependent refractive indices of the incident and the propagating medium, respectively, rearranging the grating-equation explicitly highlights the dispersive character of a grating, because θ_m directly depends on the incident wavelength λ:

$$n_1(\lambda) \cdot \sin\theta_{in} + m \cdot \frac{\lambda}{a} = n_2(\lambda) \cdot \sin\theta_m. \tag{2.3}$$

The grating-equation in this form would suggest to reconcile diffraction as an extension of Snell's refraction law, which is reproduced for $m = 0$ in Eq. 2.3. This idea was indeed recently discussed by S. Larouche and D. Smith [24], who were able to establish a formal equivalence between generalized refraction and blazed diffraction gratings.

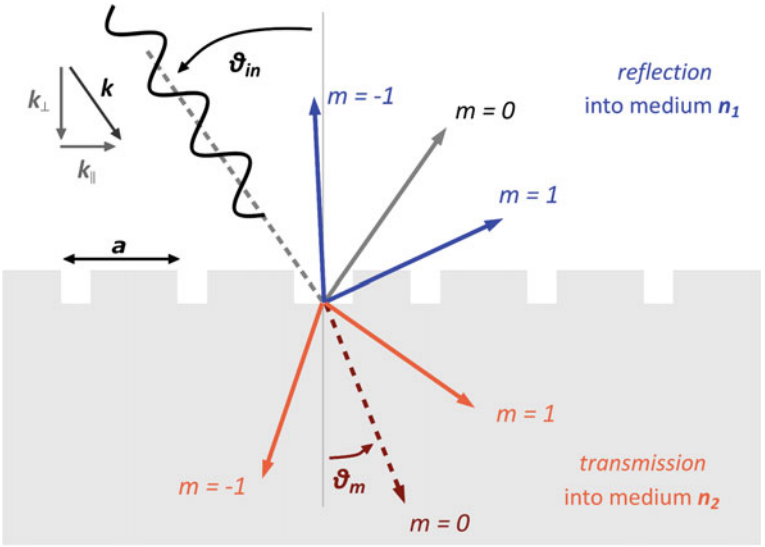

Fig. 2.5 Diffraction of an incident plane wave with wavelength λ and wave-number $k = 2\pi/\lambda$ at a structured interface layer between a medium with refractive index n_1 and medium with refractive index n_2. While k remains conserved during the interaction, diffraction requires a transfer of momentum with the grating structure. The periodicity of the grating, however, restricts the momentum transfer to integer multiples m of $2\pi/a$ and to directions within the periodic corrugations a. The important correlation between the momentum of a wave and the periodicity of a system is often explained as Bloch-theorem in solid state physics textbooks [25] and photonic crystal books [26]. The higher diffraction orders are thus the result of a stronger interaction with the periodic structure

2.2.3.2 Discussion

By assuming normal incidence $\theta_{in} = 0$, solving the grating equation for the highest diffraction order

$$|m| \leq \frac{a}{\lambda/n_2(\lambda)} \qquad \text{for} \quad \theta_m = \pi/2 \tag{2.4}$$

and for the diffraction angle θ_m, where the bijection $\arcsin(\sin x) = x$ can be applied on $x = \theta_m$, because θ_m is in the interval $(-\pi/2, +\pi/2)$ for transmission into medium n_2,

$$\theta_m = \arcsin\left(\frac{\lambda/n_2(\lambda)}{a/m}\right) \tag{2.5}$$

allows to draw the following two conclusions: although the number of diffraction orders $m(\lambda)$ scales with the grating period a (see Eq. 2.4), the diffraction angle $\theta_m(\lambda)$ drops for wavelengths $\lambda^* = \lambda/n_2$ smaller than a (see Eq. 2.5). Therefore, the more diffraction orders exist, the more light is diffracted into smaller angles.

In addition, each order only contains a small fraction of the total intensity, when the energy is spread over a continuum of diffraction orders. On the other hand, choosing

periods equal to a few wavelengths λ^* will result in more intensive, but only a few diffraction orders.

Since the lower diffraction orders tend to be more intense, a promising strategy for enhancing the absorption of light aims to shift the energy from the lower to the higher orders, as these are more likely to be totally (internally) reflected at the cladding of a silicon slab. No optical losses would result, because the energy is only redistributed amongst the diffraction orders.

In effect, this strategy strongly relies on the ability to control the phase of interfering waves. Changing the duty cycle is one example of how the absence of a diffraction order can be achieved. For example, if the ridges are half (or a third) of the grating's period, the second (or third) order will be suppressed by destructive interference.

While diffractive effects are only of minor importance in commercial solar cells today, nanophotonic structures are expected to enter the market soon. According to J. Harris (Stanford University), advisory board member from Solexel, nanodome patterns or truncated pyramids (U.S. Patent No. 8853521) are now used in commercial 40 μm thin-film silicon solar cells in order to obtain broadband and wide angle anti-reflection action. Solexel already announced the introduction of very lightweight and cheap solar modules for this year – with module efficiencies above 20 %.

2.3 The Lambertian Scatterer

In order to assess a light-trapping structure, the performance of a given design has to be benchmarked against a theoretical limit. In this section, I will analyze the model of an ideal scattering structure, called Lambertian texture, which led me to introduce the figure-of-merit described in Sect. 2.4.2.

Light is reflected or refracted (or both) at a non-structured interface, whereas a structured interface may additionally scatter the radiation into higher angular directions.

The concept of "haze" is one possible way to assess the benefits of a structured surface, because the haze value quantifies the percentage of non-refracted light. The more light is scattered, the higher the haze value would be. Consequently, more light experiences a longer path through the absorber as opposed to the situation of a non-structured interface (for which the haze value is zero). Achieving high haze over a broad range of wavelengths is therefore a desirable objective for enhancing the absorption of a thin silicon slab.

However, if the path lengths of scattered and refracted light do not differ by much, a high haze value may not necessarily translate into a higher absorption. Therefore, haze alone is not a sufficient requirement for characterising an effective light trapping structure.

A better parameter is path length enhancement: the greater the scattering angle θ, the longer the path ℓ through the absorber. I can then define the scattering efficiency in terms of the path length enhancement ℓ/d with d representing the slab thickness:

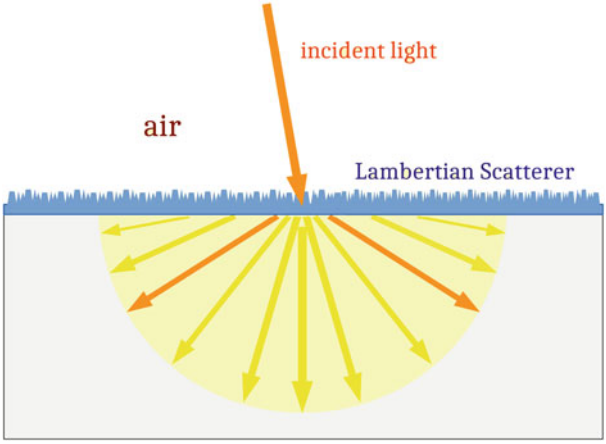

Fig. 2.6 If a scatterer radiates isotropically into a material, the light would be transmitted equally in all directions with a lobe in the shape of a hemisphere. The angular intensity distribution (AID) thereby obeyes Lambert's cosine law [28], whereas the energy will in average flow into the scattering angle $\bar{\vartheta} = \arccos\left(\frac{\cos 0° + \cos 90°}{2}\right) = \pm 60°$ (indicated by the *orange* scattered rays) independently of the the incident light, c.f. Fig. 2.9 on p. 26

$$\ell = d/\cos\theta = d \cdot \sec\theta. \tag{2.6}$$

The question of the maximum path length enhancement in a weakly absorbing slab was analyzed by E. Yablonovitch and G. Cody [27], who assumed the scattering layer to be isotropically radiating; such textures are called Lambertian, because their angular intensity distribution (AID) obeys Lambert's cosine law [28], see Fig. 2.6. The Lambertian Scatterer represents the perfect diffuser in the ray-optics approximation, with the radiated energy being understood to flow in straight lines.

The light path is defined in the framework of geometric optics. If the wavelength λ^* becomes comparable to both the absorber thickness and typical feature size of the surface Λ, near-field phenomena will modify the diffracted waves. The Frauenhofer distance $d_f = 2\Lambda^2/\lambda^*$ is a parameter often used for distinguishing the near and far-field zones from each other. Since the thickness of silicon solar cells always exceeds $d_f \approx 2\,\mu\text{m}$ and $\lambda^* \sim \Lambda$ for sunlight, the path length enhancement remains a good parameter for characterizing the scattering efficiency of a surface structure.

In the following, I will derive the absorption and the maximum path length enhancement by a Lambertian Scatterer in a different way compared to Yablonovitch and Cody, because the authors had focused only on the weak absorption regime. My derivation is based on the rarely cited idea of J. Gee [29], who had already proposed a very intuitive description of light-trapping in 1988. I generalize Gee's concept to the problem sketched in Fig. 2.7.

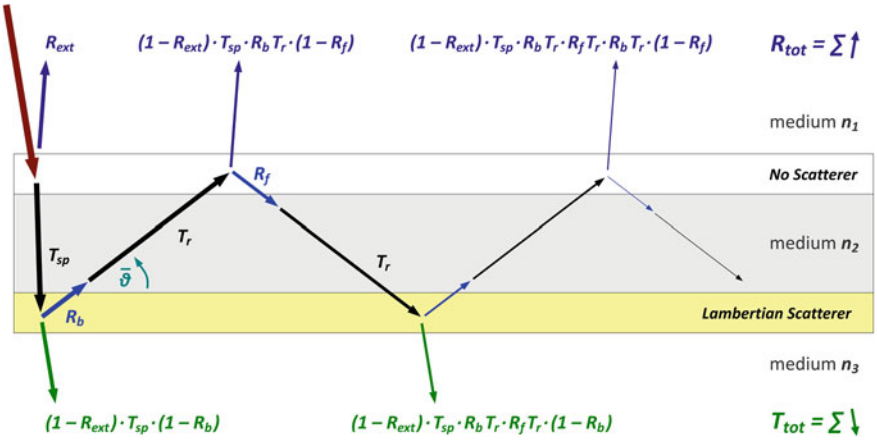

Fig. 2.7 Randomization of light at the scattering layer will allow us to neglect coherent effects, because a fixed phase relationship does not occur between diffusely-scattered, back-reflected and randomized light waves. The propagation of an averaged light ray in a lossy waveguide can then be described by the external reflection R_{ext}, the internal effective reflectances R_b and R_f and the attenuated transmission T_r with respect to the single-pass traversal T_{sp}. The total reflection R_{tot} into medium n_1 and total transmission T_{tot} into medium n_3 are therefore determined by the optical depth of the medium with refractive index n_2, the optical losses at the cladding layers and by the *angle-averaged* scattering efficiency

2.3.1 *Absorption Enhancement by a Lambertian Backscatterer*

When the Lambertian scattering layer is situated on the rear side of a slab (as in Fig. 2.7), the calculation of the photon absorption is complicated by three issues:

1. before light arrives at the scatterer, some light may already have been reflected at the surface or absorbed during the first traversal through the slab,
2. for greater scattering angles θ, less light will fall into the escape cone, defined by the critical angle θ_c of total internal reflection,
3. the angular intensity distribution (AID) follows Lambert's cosine law only if the slab becomes transparent.

I can cover the first issue by truncating the incident spectrum on the Lambertian texture, considering the external reflection air/Si and the absorption of the first traversal through the slab, as shown in Fig. 2.7.

By calculating the angle-averaged (internal) Fresnel reflection $R_f(\lambda)$ at the front interface, assuming rotational symmetry, I can effectively address the second point:

$$R_f(\lambda) \equiv \frac{1}{\pi}\int R_f(\lambda,\theta)\,\vec{n}\cdot d\vec{\Omega} \tag{2.7}$$

The more light is back-scattered from the surface normal $\vec{n}$ into the differential solid angle $d\vec{\Omega}$ of a hemisphere, the higher the effective front reflection will be. The normalization factor $1/\pi$ is required by energy conservation, e.g. consider the case of an angular-independent reflectance $R_f(\theta) = const.$:

$$\begin{aligned} R_f(\lambda) \;&\equiv\; \frac{1}{\pi}\int R_f(\lambda,\not{\theta})\,\vec{n}\cdot d\vec{\Omega} \;=\; \frac{R_f(\lambda,\not{\theta})}{\pi}\int |\vec{n}|\;|d\vec{\Omega}|\;\cos\theta \\ &=\; \frac{R_f(\lambda)}{\pi}\int_0^{2\pi} d\varphi \int_0^{\pi/2} \cos\theta\cdot\sin\theta\, d\theta \\ &=\; R_f(\lambda)\cdot\int_0^{\pi/2} (2\,\sin\theta\,\cos\theta)\, d\theta \;=\; R_f(\lambda)\cdot\left[\sin^2\theta\right]_0^{\pi/2} \;=\; R_f(\lambda). \end{aligned}$$

For a material with an high refractive index and small escape cone

$$\begin{aligned} R_f(\lambda) \;&\equiv\; \frac{1}{\pi}\int R_f(\lambda,\theta)\,\vec{n}\cdot d\vec{\Omega} \\ &=\; \int_0^{\pi/2} R_f(\lambda,\theta)\;(2\,\sin\theta\,\cos\theta)\cdot d\theta \;=\; \int_0^{\pi/2} R_f(\lambda,\theta)\;\sin(2\theta)\cdot d\theta \\ &=\; \int_{\theta_c}^{\pi/2} \underbrace{R_f(\lambda,\theta)}_{=\,1}\;\sin(2\theta)\cdot d\theta \;+\; \int_0^{\theta_c} R_f(\lambda,\theta)\;\sin(2\theta)\cdot d\theta \\ &=\; 1-(\sin\theta_c)^2 \;+\; \int_0^{\theta_c} R_f(\lambda,\theta)\;\sin(2\theta)\cdot d\theta, \end{aligned} \tag{2.8}$$

the last term may be negligible. For total internal reflection, $\sin\theta_c$ in Eq. 2.8 can be further replaced by the ratio of the refractive indices of the interfacing materials, according to Snell's refraction law Eq. 2.3 (for $m = 0$).

The third point is easily violated in the presence of coherent effects (resonances), yet it is quite reasonable to assume incoherent scattering for a perfect diffuser. This assumption allows me to proceed with a statistical ray optics approach, where the light-paths are completely randomized and the phase information lost.

As most backscattered light rays will differ in their path through the slab of thickness d, sometimes authors have used the angle-averaged path length $\bar{\ell} = d\cdot\sec\bar{\theta}$ for the calculation of the randomized transmission T_r:

$$T_r(\alpha,\bar{\theta}) \;=\; e^{-\alpha\bar{\ell}} \;=\; \left(T_{sp}\right)^{\sec\bar{\theta}}, \tag{2.9}$$

where α stands for the wavelength-dependent absorption coefficient and T_{sp} for the transmission of a non-randomized single pass traversal through the slab. In the literature, the exponential factor $a = \sec\bar{\theta}$ is also known as the Lambertionality factor [30]. However, when I properly take into account that the radiance of each propagating light ray is reduced by a factor of $e^{-\alpha d\cdot\sec\theta}$

$$T_r(\alpha d) \equiv \int_0^{\pi/2} e^{-\alpha d\cdot\sec\theta}\,\sin(2\theta)\cdot d\theta \tag{2.10}$$

and set Eq. 2.9 equal to Eq. 2.10, I can express $\bar{\theta}$ as a function of the absorption coefficient:

$$\begin{aligned} T_r(\alpha d) \;&=\; \int_0^{\pi/2} e^{-\alpha d\cdot\sec\theta}\,\sin(2\theta)\cdot d\theta \;\overset{!}{=}\; \left(T_{sp}\right)^{\sec\bar{\theta}} \\ \Rightarrow\quad & \frac{\ln T_{sp}}{\ln T_r} \;=\; \cos\bar{\theta} \;\geq\; 0 \qquad \text{since}\quad \left|\bar{\theta}\right| \;\leq\; 90^\circ \\ \Rightarrow\quad & \bar{\theta}(\alpha(\lambda), d) \;=\; \arccos\frac{-\alpha(\lambda)\,d}{\ln\left(\int_0^{\pi/2} e^{-\alpha(\lambda)d\cdot\sec\theta}\,\sin(2\theta)\cdot d\theta\right)}. \end{aligned} \tag{2.11}$$

Since the scattering angle $\bar{\theta}$ indicates the average flow direction of energy from the scatterer into the absorber slab as illustrated in Fig. 2.6, $\bar{\theta}$ depends on the absorber's material properties and thus can not be defined a priori to calculate the transmitted intensity via Eq. 2.9, i.e. $T_r \;\Rightarrow\; \bar{\theta}$.

For example, if all the incident energy were scattered into an angle $\bar{\theta}$, the angular intensity distribution (AID) of the Lambertian Scatterer would be replaced by a small lobe. The statistical nature of the Lambertian model will then be misinterpreted, because a Lambertian Scatterer spreads the incident light into a full hemisphere.

The graph in Fig. 2.8 now demonstrates that the average scattering angle of a Lambertian diffuser drops in the presence of absorption for shorter wavelengths; this drop is not due to imperfect randomization of the incident light by the scatterer, but due to the loss of isotropy of the scattered radiation due to absorption, which equally leads to a deviation from Lambert's cosine law.

In conclusion, the radiance of a Lambertian Scatterer becomes anisotropic in absorbing media, such that it would be misleading to assume the average-scattering angle $\bar{\theta}$ or the average path length $\bar{\ell}$ as independent of the material properties. From the point of view of scattering, a structure then should not be optimized for a thin absorber layer or for the weak absorption regime only, but for optical depths greater than 0.01 dB.

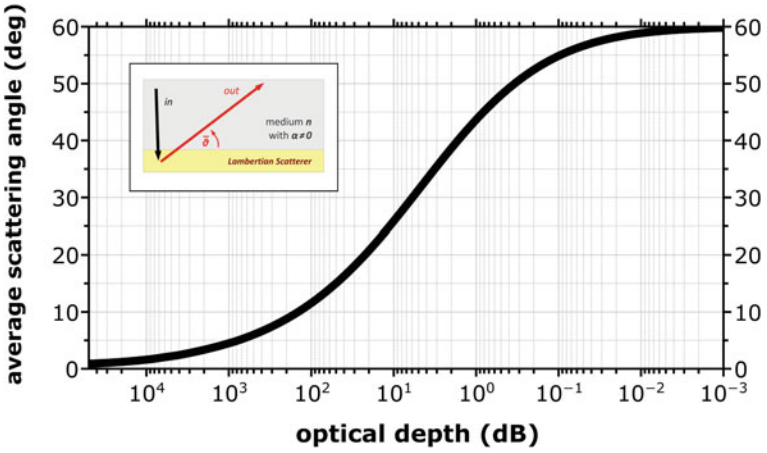

Fig. 2.8 The average scattering angle $\bar{\theta}$ specifies the average direction of the radiated energy flowing into a medium with refractive index n and thickness d. The angular intensity distribution (AID) of a Lambertian diffuser, however, can deviate from the cosine law in presence of absorption $\alpha \neq 0$. The radiance then looses its isotropic character, because the energy flow is less attenuated for rays that are scattered into smaller angles. In Sect. 1.3.1, I defined the optical depth of 0.01 dB as the medium's threshold value for transparency. A Lambertian Scatterer thus will scatter Lambertianly only, when the optical depth falls below 0.01 dB, i.e. when the product of α and d is smaller than 0.003 – which stands in contrast to a wavelength independent scattering angle $\bar{\theta}(\not\lambda)$ or the constant Lambertionality factor $a(\not\lambda) = \sec\bar{\theta} = const.$ by Battaglia et al. [30]. Please note that the Yablonovitch and Cody treatment assumes a constant angle of 60°, so especially for strongly absorbing media, this angle may be very different form the effective angle shown here

2.3.1.1 The Lambertian Limit

In the following I will derive the total absorption of a slab with a Lambertian Scatterer at the back or front side. Since the outlined derivation is based on the multiple reflections at the cladding layers, the only required quantities to know are (a) the optical depth of the absorber slab and (b) the refractive index contrast between the absorber and the incident or substrate medium. I will first calculate the absorption caused by the randomization of the light-paths through the slab, i.e. T_r, and afterwards account for the multipass nature of trapped light. The integral in Eq. 2.10 is evaluated with the help of the exponential integral

$$\Gamma(\tau) = \int_{\tau}^{\infty} \frac{e^{-u}}{u} \cdot du,$$

the substitution $u(\theta) = \tau/\cos\theta$ and two integrations by parts:

$$\begin{aligned} T_r(\tau \equiv \alpha\, d) &= \int_0^{\pi/2} e^{-\tau/\cos\theta} \sin(2\theta) \cdot d\theta = 2\tau^2 \cdot \int_\tau^\infty \frac{e^{-u}}{u^3} \cdot du \\ &= 2\tau^2 \cdot \left(\frac{e^{-\tau}}{2\tau^2} - \frac{1}{2} \int_\tau^\infty \frac{e^{-u}}{u^2} \cdot du \right) \\ &= e^{-\tau} - \tau^2 \cdot \left(\frac{e^{-\tau}}{\tau} - \Gamma(\tau) \right) \\ &= e^{-\tau}(1 - \tau) + \tau^2 \cdot \Gamma(\tau), \end{aligned} \tag{2.12}$$

and does only depend on the optical depth $\tau = \alpha d$, which is the product of the wavelength dependent absorption coefficient α and the physical thickness of the slab d. Finally, the total absorption A_{tot} of a slab with Lambertian back-scatterer can now be calculated by adding all reflected and transmitted light paths together like it was illustrated in Fig. 2.7:

$$\begin{aligned} A_{tot} &= 1 - R_{tot} - T_{tot} \\ &= 1 - \left(R_{ext} + \sum_{m=0}^{\infty} (1 - R_{ext}) \cdot T_{sp}\, R_b T_r \cdot (R_f T_r\, R_b T_r)^m \cdot (1 - R_f) \right) \\ &\quad - \left(\sum_{m=0}^{\infty} (1 - R_{ext}) \cdot T_{sp} \cdot (R_f T_r\, R_b T_r)^m \cdot (1 - R_b) \right) \\ &= (1 - R_{ext}) - \frac{(1 - R_{ext}) \cdot T_{sp}}{1 - R_b R_f T_r^2} \cdot \left[R_b T_r \cdot (1 - R_f) + (1 - R_b) \right] \\ &= \frac{(1 - R_{ext})}{1 - R_b R_f T_r^2} \cdot \left[\left(1 - R_b R_f T_r^2 \right) - T_{sp}\, R_b T_r (1 - R_f) - T_{sp}(1 - R_b) \right] \\ &= \frac{1 - R_{ext}}{1 - R_b R_f T_r^2} \cdot \left[(1 - T_{sp}) + (1 - T_r) \cdot R_b T_{sp} + (T_{sp} - T_r) \cdot R_b R_f T_r \right]. \end{aligned} \tag{2.13}$$

R_{ext} stands for the probability that an incident photon is reflected by the slab, whereas $T_{sp} \geq T_r$ is the transmitted fraction after the first direct traversal. The prefactor (recirculation factor) takes into account the attenuation of the average light ray due to the multiple upward and downward reflections at the cladding layers. The specular case is reproduced for $T_r = T_{sp}$, i.e. when the single pass absorption $(1 - T_{sp})$ is enhanced by the product of R_b and T_{sp}. If the Lambertian Scatterer is designed to work in transmission, T_{sp} must be replaced by T_r, which maximizes the total absorption A_{tot}.

The effective backreflection R_b is 100 % only for a lossless reflecting surface and may otherwise be analogously defined to R_f in Eq. 2.7:

$$R_b(\lambda) \equiv \frac{1}{\pi} \int R_b(\lambda, \theta)\, \vec{n} \cdot d\vec{\Omega}. \tag{2.14}$$

The more light is back-scattered from the surface normal $\vec{n}$ into the differential solid angle $d\vec{\Omega}$ of a hemisphere, the higher the effective back reflection R_b will be. A black substrate, for example, would reflect almost no incident radiation ($R_b = 0$) back into the absorber layer; a silver mirror is instead highly reflective ($R_b > 95\,\%$) for wavelengths above 800 nm, yet highly absorptive ($R_b < 90\,\%$) for wavelengths below 500 nm.

Since Eqs. 2.14 and 2.7 allow us to calculate R_b and R_f for arbitrary substrate and incident media, respectively, Eq. 2.13 can be used to calculate the absorption enhancement by a Lambertian Scatterer on the bottom or top (with $T_{sp} = T_r$) of absorber layers.

2.3.2 The Maximum Absorption Enhancement

The multipass nature of the Lambertian model is highlighted by the absorption enhancement due to the randomization of the path lengths. Dividing Eq. 2.13 by the absorption of a direct traversal $1 - T_{sp}$ allows to quantify the enhanced absorption:

$$\begin{aligned}
\frac{A_{tot}}{1 - T_{sp}} &= \frac{1 - R_{ext}}{1 - R_b R_f T_r^2} \cdot \left[\left(\frac{1 - T_{sp}}{1 - T_{sp}} \right) + \left(\frac{1 - T_r}{1 - T_{sp}} \right) \cdot R_b T_{sp} + \right. \\
&\qquad \left. + \left(\frac{T_{sp} - 1 + 1 - T_r}{1 - T_{sp}} \right) \cdot R_b R_f T_r \right] \\
&= \frac{1 - R_{ext}}{1 - R_b R_f T_r^2} \cdot \left[1 + \left(\frac{1 - T_r}{1 - T_{sp}} \right) \cdot R_b T_{sp} + \left(\frac{1 - T_r}{1 - T_{sp}} - 1 \right) \cdot R_b R_f T_r \right] \\
&= \frac{1 - R_{ext}}{1 - R_b R_f T_r^2} \cdot \left[1 + \eta \cdot R_b T_{sp} + (\eta - 1) \cdot R_b R_f T_r \right].
\end{aligned} \tag{2.15}$$

Since $T_r \leq T_{sp}$ (see Eq. 2.12), the enhancement factor describing randomisation alone, which can be expressed as

$$\eta(\tau \equiv \alpha\, d) = \frac{1 - T_r}{1 - T_{sp}} = 1 + \frac{\tau}{1 - e^{-\tau}} \cdot \left[e^{-\tau} - \tau \cdot \Gamma(\tau) \right], \tag{2.16}$$

is at best equal to 2 for weakly absorbed light ($\tau \to 0$), while it is unity for strongly absorbed light ($\tau \to \infty$), since the limit of the function $\tau \cdot \Gamma(\tau)$ is zero for both cases. The $4n^2$ absorption enhancement limit derived in Ref. [27] can then simply

be reproduced in first order approximation for $R_{ext} = 0,\ R_b = 1$ and $R_f \approx 1 - 1/n^2$, with n being the refractive index of the medium:

$$\frac{A_{tot}}{1 - T_{sp}} \approx \frac{1 - 0}{1 - (1 - 1/n^2)} \cdot \left[1 + 2 \cdot 1 + 1 \cdot (1 - 1/n^2)\right] = 4n^2 - 1. \tag{2.17}$$

The theoretical maximum absorption enhancement is reduced by the first direct traversal, because the $4n^2$ limit corresponds to a Lambertian front-scatterer with T_r replacing T_{sp} in Eq. 2.13.

In reference to Eq. 1.1, I see light-trapping as the ability to increase the intensity by $2\,n^2$ and the optical depth $\tau = \alpha d$ of a medium by *two on average*, at best:

$$\left(2 \cdot n^2\right) \cdot (2 \cdot \tau) \ = \ 4n^2 \cdot \alpha d. \tag{2.18}$$

Since the photon absorption is proportional to the incident photon flux, i.e. to the product of the photon density $\propto n^3$ and the group velocity $\propto c/n$, the enhancement of n^2 is due to the medium effect (brightness theorem).

The n^2 enhancement rests on the assumption of an equilibrium between the incident black-body illumination and the internal isotropic radiation field. For a perfect mirror at the backside of the thin-film, the enhancement factor is further increased by a factor of 2, because the incident light intensity is virtually doubled. Scattering thus aims to maximize the optical depth τ.

For a Lambertian scatterer, the average path length $\bar{\ell}$ through a slab is exactly twice the slab thickness:

$$1 - T_r \ \approx \ \alpha \cdot \bar{\ell} \ = \ \int_0^{\pi/2} (\alpha d \cdot \sec\theta) \cdot \sin(2\theta) \cdot d\theta \ = \ \alpha \cdot (2d) \tag{2.19}$$

as long as $\alpha d < 0.01$ dB. Consequently, light is mostly scattered into the angle $\bar{\theta} = 60°$ in this weak absorptive regime, as illustrated in Fig. 2.9.

If a scatterer is able to achieve $\bar{\ell} = 2d$ even in presence of absorption, it would outperform the Lambertian case, whereas a scatterer with $\bar{\ell} > 2d$ will beat the $4n^2$ limit. Curiously, authors sometimes assume a Lambertian texture, but then consider *all* path lengths to be enhanced by $4n^2$,

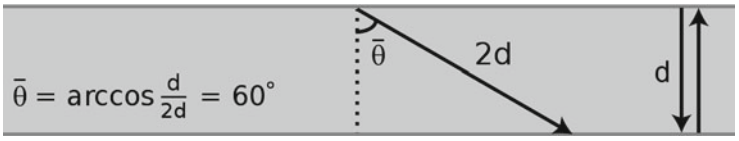

Fig. 2.9 If light is scattered into the angle $\bar{\theta}$ and traverses the absorber layer as it were twice as thick, the scattering angle will be $\bar{\theta} = 60°$

$$A_{max} \equiv 1 - \exp\left(-\alpha \cdot 4n^2\, d\right) \approx \frac{4n^2 \cdot \alpha\, d}{1 + 4n^2 \cdot \alpha\, d} \qquad \text{for } \alpha\, d < 0.01 \text{ dB}, \quad (2.20)$$

which does misrepresent the physical picture. The comparison may still be adequate, as effectively the analogy was made between a textured slab and a $4n^2$ times thicker unstructured absorber layer. However, A_{max} in Eq. 2.20 will overestimate A_{tot} in Eq. 2.13 for $\alpha d > 0.01$ dB, i.e. when the angular intensity distribution (AID) falls below Lambert's cosine law.

2.3.2.1 Over the Limits

If interference effects violate the ray approximation, it becomes difficult to define an optical path length. The efficiency of a photonic structure must then be reformulated as its ability to enhance the optical depth of a thin film [31].

Assuming a silicon slab can be understood as an optical waveguide, Yu et al. [32] explain why the $4n^2$ limit remains valid over a large spectral bandwidth.

The authors first compare the available number of propagating waveguide modes in each wavelength interval with the ability of a scatterer to couple sunlight in or out of these modes. The integrated absorption thereby serves as a figure of merit in this comparison, because a strong coupling is generally seen as incompatible with a large bandwidth. The outcome of the comparison then shows that the number of available modes directly scales with the absorber thickness, whereas the correlated coupling strengths are only subject to the design of the surface structure. Therefore, the maximum integrated absorption enhancement becomes independent of the absorber thickness when compared to the single-pass absorption.

Secondly, the authors demonstrate how a strong spectral dependency of periodic structures allows to achieve enhancement factors above $4n^2$ in limited wavelength ranges. However, reducing the operating bandwidth does not maximize the integrated absorption, because the absorption would drop in other spectral regions.

Finally, Yu et al. also highlight the effect of a strong angular dependency. If Θ_{in} is the limiting angle of incidence with respect to the normal to the surface, the coupling strength is proven to scale with $1/\sin^2\Theta_{in}$. Absorption enhancement factors can therefore be as high as $4n^2/\sin^2\Theta_{in}$, when the surface structure is designed to address only a selected range of incident angles. In fact, the $4n^2$ limit was derived on the assumption of an acceptance cone covering the full hemisphere ($\Theta_{in} = 90°$), as mentioned in Fig. 2.6.

In conclusion, since efficient solar cell operation requires a broad angular and spectral response to sunlight, the $4n^2$ absorption enhancement remains the limiting case for stationary solar cells. Higher enhancement factors may be possible in a limited wavelength range, but also reduce the total integrated absorption.

Peters [33] was recently able to derive the same conclusion than Yu et al., yet his study only based on the conditions of how light is incident onto and escapes from an isotropic absorber. Therefore, the $4n^2$ absorption enhancement factor is not a specific

fundamental limit for diffractive light-trapping structures, but applies independently of the scattering mechanism.

2.4 Assessment of Light-Trapping

Many research proposals show large absorption enhancement factors or claim to have achieved the $4n^2$ limit. However, the assessment of the light-trapping technique itself turns out to be difficult, because proposals often differ from each other either in the design or in the operating spectral and angular range.

In the end, I may get guidance from simulations of which geometries or features are desirable and from measurements indicating real performances. A quantitative assessment is further complicated by the vast diversity of methods used, which include anti-reflection and in-coupling concepts, 1D and 2D back-scatterers, embedded metal nanoparticles, photonic crystals and random or periodic diffractive structures on one or one both sides of the absorber layer. Since all of these methods are applied to different materials and layer thicknesses, it seems difficult to define a figure-of-merit that can purely assess the performance of a light-trapping technique – irrespective of the material, fabrication method and technology used.

2.4.1 How to Assess Light-Trapping Structures for Solar Cells ?

Light-trapping is commonly assessed by the absorption enhancement compared to a flat silicon slab, so a common figure-of-merit is the ratio of the absorption A_{max} of a structured slab to the absorption A_{ref} of an unstructured reference slab:

$$F \equiv \frac{\int A_{\mathrm{max}}(\lambda) \cdot \mathrm{d}\lambda}{\int A_{\mathrm{ref}}(\lambda) \cdot \mathrm{d}\lambda}. \tag{2.21}$$

Since the enhancement factor F is maximal in the weak-absorption regime, i.e. when the optical depth is in the order of some centi-dBs, many studies cited enhancements factor only for this regime. However, light-trapping for photovoltaic applications aims to increase the absorption over the full wavelength range of the solar spectrum, i.e. from 300 nm up to the wavelength bandgap λ_{max} of the absorber material, so such high enhancement factors have little practical utility.

Instead, the quantity directly related to the integrated total absorption is the generated electrical current of a solar cell. If there was no voltage drop, the short-circuit current J_{sc} would be the largest current which may be drawn from a solar cell. Therefore, light-trapping might be assessed in terms of the J_{sc} enhancement compared to a non-structured reference:

$$F^* \equiv \frac{J_{max}}{J_{ref}} = \frac{\int_{300\,\mathrm{nm}}^{\lambda_{max}} A_{\mathrm{max}}(\lambda)\,\Phi(\lambda)\cdot \mathrm{d}\lambda}{\int_{300\,\mathrm{nm}}^{\lambda_{max}} A_{\mathrm{ref}}(\lambda)\,\Phi(\lambda)\cdot \mathrm{d}\lambda}. \tag{2.22}$$

Here, Φ is the photon flux of the standard reference spectrum AM1.5G, which is the solar spectrum most articles refer to.

However, the figure-of-merit F^* would not distinguish between the causes of the current enhancement, because a higher enhancement factor F^* could be achieved by a different anti-reflection coating or by a difference in absorber material quality.

In order to eliminate the material quality dependence, proposals have been benchmarked against the material dependent Lambertian enhancement factor J_{LL}/J_{ref}:

$$G \equiv \frac{F^*}{J_{LL}/J_{ref}} = \frac{J_{max}}{J_{LL}}, \tag{2.23}$$

which expresses the performance of the proposed structure J_{max} against the theoretical achievement J_{LL} of a Lambertian texture. Therefore, the G factor quantifies the electrical current in percentages of an ideal Lambertian texture.

For a few common photovoltaic materials, Bozzola et al. [31] reported the ideal short-circuit current J_{ref} achieved with an unstructured slab against the theoretical maximum short-circuit current J_{LL} achieved by a Lambertian texture as a function of the absorber thickness (exemplary shown in Fig. 2.10 for silicon). Their study graphically illustrates not only how the G factor depends on the absorber thickness, but also why the G factor rather impedes the assessment of light-trapping. For example, even a non-structured solar cell yields a $G > 0$ or can approach $G = 1$, because the current generated by only a double pass traversal of light can be as high as 40 mA/cm^2 in a 100 µm thick silicon absorber layer, i.e. $G = 40/45 \approx 0.9$ according to Fig. 2.10.

Basch et al. [34] were the first to propose a thickness and material independent figure-of-merit that tried to isolate the light-trapping effect as much as possible. They suggested to compare the current gain by a proposed texture $J_{max} - J_{ref}$ against the theoretical gain by a Lambertian texture $J_{LL} - J_{ref}$:

$$G^* \equiv \frac{J_{max} - J_{ref}}{J_{LL} - J_{ref}} = \frac{G \cdot J_{LL} - J_{ref}}{J_{LL} - J_{ref}} \tag{2.24}$$

If subtracting the current J_{ref} of a non-structured solar cell from the current J_{max} of a structured solar cell removes the contribution provided by anti-reflection, G^* would only quantify the benefits of the light-trapping technique.

However, the theoretical model of a Lambertian texture assumes a scattering layer of zero thickness. The anti-reflection effect of a Lambertian texture can thus take any arbitrary value. While ideal anti-reflection properties are generally assumed for the calculation of J_{LL}, practically, anti-reflection coatings will hardly cover the full solar spectrum. Therefore, if the denominator in Eq. 2.24 underestimates the

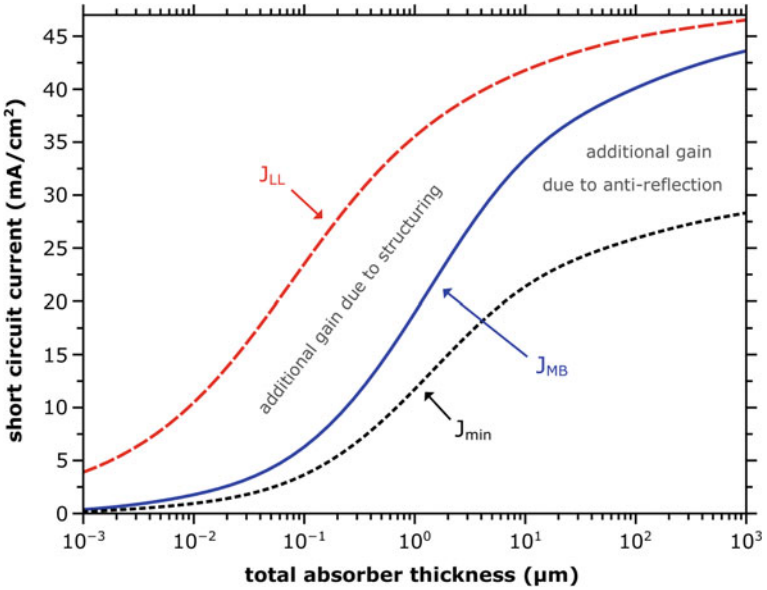

Fig. 2.10 In contemporary solar cell research, the figure of merit is often identified with the improvement in the short-circuit current. In the figure above, the short-circuit current density J_{sc} for crystalline silicon is expressed as a function of the absorber layer thickness (assuming the AM 1.5 global solar spectrum). The J_{MB} and J_{min} graphs correspond to currents generated by a double pass traversal of light in the absorber layer with (*blue solid*) and without (*black dotted*) perfect anti-reflection coating, respectively. The J_{LL} refers to devices textured with an ideal Lambertian scatterer and perfect anti-reflection coating (*red-dashed line*). All devices have a perfect mirror on the back. Please note that the *red* and the *blue curves* will converge for thicknesses greater than 10^4 μm due to the indirect nature of silicon's bandgap. For example, while the global solar irradiance is still more than 25 % of its peak value at 1280 nm wavelength, a 1,000 μm thick silicon absorber does only absorb 20 % of it by a double pass traversal of light, whereas a ten times thicker layer can already absorb 90 % of it

anti-reflection properties of the reference cell, the G^* factor will always remain smaller than 1. In order to achieve a $G^* = 1$, the proposed structure will need to either provide additional anti-reflection action apart from Lambertian light-trapping or it needs to outperform the performance of a Lambertian texture – the meaning of G^* then remains ambiguous.

Pratesi et al. [35] defined a similar G^* factor, but only suggested to replace J_{LL} in the denominator of Eq. 2.24 with the *total incident photon-flux* of the sun J_{sun} (expressed as an electrical current). This substitution would therefore not change any conclusions of the previous discussion regarding the format of the figure-of-merit, as the denominator will still not properly take the anti-reflection properties into account. In fact, the proposed figure-of-merit rather highlights the impossibility to achieve a $G^* = 1$, because the current J_{max} of a structured solar cell would now

need to absorb all incident photons from sun, whereas semiconductors are transparent to photons whose energies lie below their bandgap.

2.4.2 The Light-Trapping-Efficiency (LTE)

I proposed to replace J_{ref} in the denominator of Eq. 2.24 by the short-circuit current J_{MB} of an ideal reference device.

$$LTE \equiv \frac{J_{max} - J_{ref}}{J_{LL} - J_{MB}}. \tag{2.25}$$

Since J_{LL} and J_{MB} assume perfect anti-reflection at the illuminated surface on the front and perfect reflection at an ideal metal mirror on the back of the absorber layer, the current gain $J_{LL} - J_{MB}$ purely reflects the light-trapping capability of a Lambertian texture. Therefore, the *LTE* separates the anti-reflection action from light-trapping, because it compares the real gain by structuring (nominator) to the hypothetical gain of ideal devices (denominator).

The format also follows the efficiency η_c of a Carnot heat-engine, which compares the amount of entropy-free energy delivered to a load (nominator) against the ideal case (denominator) with the removal of all thermal energy Q:

$$\eta_c = \frac{Q_{max} - Q_{ref}}{Q_{max} - 0}. \tag{2.26}$$

In order to maximize the efficiency of a Carnot-engine, the heat sink Q_{ref} in Eq. 2.26 would need to suspend all thermal motions and interactions. Correspondingly, in order to take advantage of light-trapping, J_{ref} would need to be as close as possible to J_{MB} in Eq. 2.25. Starting from a good reference device is thus as important as making a good light-trapping structure; otherwise, using a different anti-reflection coating layer could become more beneficial than light-trapping.

The format of the *LTE*, however, seems to allow a higher figure-of-merit with the degree of worsening the reference device J_{ref}. Viewed optically, J_{ref} will always consist of a coating layer, which could just be the encapsulation layer for protecting the solar cell from moisture, in addition to a back-reflector for enhancing the photon flux in the absorber medium. It is true, that both techniques, in reality, do not work over a broad bandwidth without any optical losses; anti-reflection coatings are not 100 % transmissive as mirrors are not 100 % reflective for all photonts. Therefore, once the optimized coating and back-reflector were applied, the same coating and mirror must also be applied to the structured solar cell device. Any reduction of J_{ref} would then likewise affect J_{max}, such that $J_{max} - J_{ref}$ purely highlights the benefit of the structuring approach.

Secondly, since the material properties of J_{ref} also determine J_{MB} and J_{LL}, the *LTE* remains independent of the material properties and only assesses the light-trapping

capability J_{max}. A $LTE = 1$ then means, that a structure achieved the same current gain as a Lambertian scatterer – irrespective of the method or technique used.

2.4.2.1 The Effective Thickness

The absorption in Eq. 2.13 was defined as a function of the total absorber layer thickness, assuming the Lambertian scatterer to be of vanishing thickness. Therefore, all calculated short-circuit currents shown in Fig. 2.10 refer to the total thickness t_{tot} of the silicon slab.

Since the absorption enhancement is also thickness dependent, I need to consider what thickness value to use for a structured material. Should I use the maximum thickness, i.e. the thickness between the bottom of the film and the peaks of the structure, or should I use some effective thickness t_{eff} that represents the equivalent volume of material?

The effective-thickness t_{eff}, which is the average thickness of the material, is often seen as a figure-of-merit for the greatest possible absorption achieved with the least volume of material. The most promising literature proposals might then be those with the smallest effective-thickness t_{eff}.

However, the effective-material-thickness t_{eff} should not be confused with the effective-optical-thickness $\bar{\ell}$ defined by Eq. 2.9, which is the angle-averaged path length through the absorber; it is $t_{eff} \leq \bar{\ell} \leq 2\,t_{tot}$ (see Eq. 2.19).

The *LTE* in Eq. 2.25 is defined for the total thickness t_{tot} of the absorber that includes the scattering layer, as was shown in Fig. 2.11. Therefore, the *LTE* does not take the material consumption into account.

The effective material thickness seems to be a useful concept for comparing light trapping structures in terms of their material budget, but the performance of a scatterer depends not only on the volume of the absorber material V_{Si} or on the geometry of the structure. The volume of material in between the structures V_{cm} plays an equally important role, as it determines the refractive index contrast and thus the scattering efficiency. Since t_{eff} always neglects the volume contribution of the complementary material V_{cm}, it consequently lowers the Lambertian limit of absorption:

$$t_{eff} \equiv \frac{V_{Si}}{A} < \frac{V_{Si} + V_{cm}}{A} \equiv t_{tot}, \tag{2.27}$$

where A stands for the illuminated surface area of the active absorber. To illustrate, if I was to construct an absorber layer of 1 μm thickness with narrow pillars of 4 μm height, the effective thickness might only be $t_{eff} = 1.2\,\mu m$, which makes for a very favourable comparison. Instead, I believe that one should use $t_{tot} = 5\,\mu m$, as the scattering layer adds 4 μm to the absorber layer of 1 μm.

Ultimately, very narrow and high aspect-ratio structures, such as the long nanowires in Fig. 2.12a, mainly aim to maximize the surface-to-volume ratio. The higher the aspect-ratio, the larger the surface area and the more often a photon will interact with the structure, even though it may already entered and left the absorber material

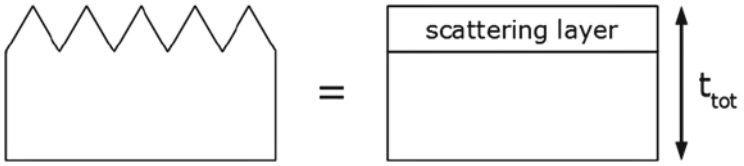

Fig. 2.11 The performance of a scatterer relies on the refractive index contrast and thus on the materials between the structures. Therefore, the LTE is defined for the total thickness t_{tot} of the absorber material that includes the scattering layer

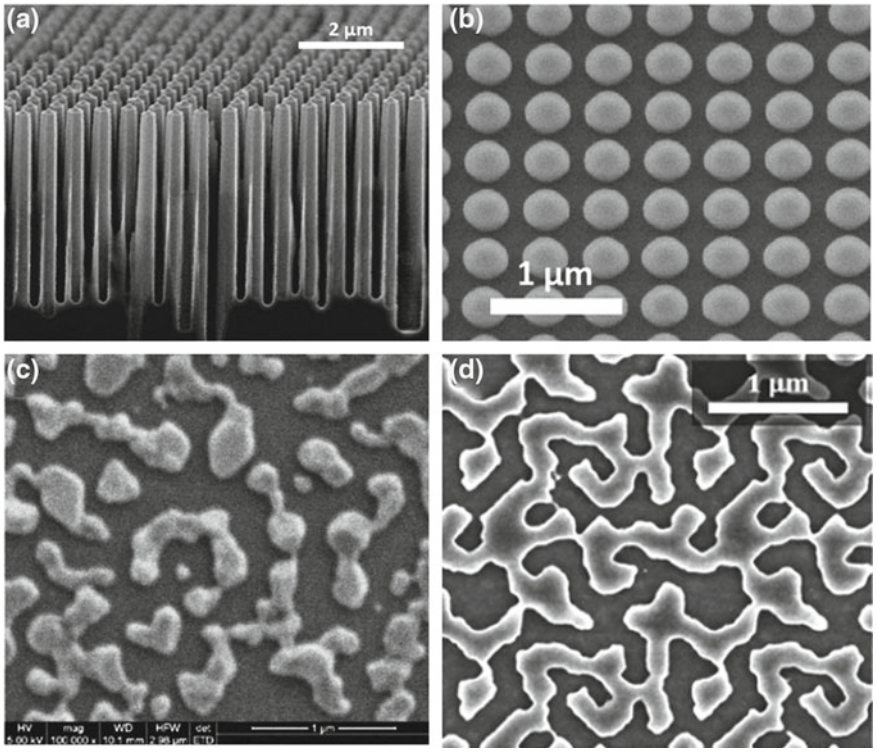

Fig. 2.12 Long silicon nanowires (4 µm long) and arrays of small nanopillars (150 nm high) have both shown to yield excellent anti-reflective properties. While the high-aspect ratio of closely spaced silicon nanowires (**a**) notably reduces the external back-reflection [16], dielectric Mie-scatterers (**b**) are able to strongly enhance the coupling efficiency of incident light into the absorber layer [14]. The Mie resonance of metallic nanostructures may in principal be superior to dielectric scatterers, given the high polarizability of localized plasmonic particles. In practice, however, the parasitic losses tend to almost compensate the benefit of the plasmonic scatterers. Please note that the best performing plasmonic structure in [17], here shown as image (**c**), looks quite similar to one of my own best performing diffractive textures, here shown as image (**d**), which made me wondering about the mechanism of the improved light trapping performance

before – hence the higher its absorption probability for the same effective thickness t_{eff}. The *LTE*, however, does not assess the interaction rate *with* the structure, but aims to assess the longer dwell time a photon spends in the absorber material *due to* a light-trapping structure, correctly addressed by the total absorber thickness t_{tot}.

2.5 State of the Art

Before I will apply the *LTE* of Eq. 2.25 to literature proposals, a few important milestones that paved the way for thin-film silicon solar cell technology are reviewed. The survey in Sect. 2.5.1 covers the important milestones that guided the advancement in our technical understanding. The current state-of-the-art is summarized in Sect. 2.5.2. Finally, as I was indeed able to identify a few structures very close to a light-trapping efficiency equal to $LTE = 1$, I will analyze their common aspects in Sect. 2.6.

2.5.1 Important Milestones

Even if the genesis of photovoltaics can be traced back to the observations by E. Becquerel in 1839, progress in photovoltaics has been slow and has proceeded in approximately half-century steps.

The discretization of light in 1900 by M. Planck is often referred to as the foundation of quantum theory. The theory was not only able to explain why a metal plate can eject electrons under the action even very low intensity light (photoelectric effect), but also provided the framework for the realisation of the first silicon solar cell in 1946 by Ohl [36] and the point-contact transistor in 1947 by Shockley et al. [37].

In fact, the pioneering work by W. Shockley marked the invention of the pn-junction diode and the first practical silicon solar cell shortly after. Although the device was a milestone in the history of photovoltaics with a 6 % power conversion efficiency, this success is only humbly reported in a very short letter by Chapin et al. in 1954 [38]. The reason may have been that Texas Instruments was already in the leverage position to manufacture silicon pn-junctions in volume [39], owing to G. Teal's technical achievement of silicon purification and crystal growth [40].

By the end of the 50s, silicon thus began to replace the industry's preferred semiconductor material, germanium, yet it took another half-century for a silicon photovoltaic industry to emerge.

The oil crisis of the 70s kick-started interest in solar power for terrestrial use. Competing with a large solar program in the USA, M.A. Green started the solar laboratory at the University of New South Wales in 1974. His research team soon became internationally recognized as one of the elite in the field; the group frequently set new world-record efficiencies by improved electrical and optical designs. For example, the first 20 % efficient cell was fabricated by the group in 1985 [41] and

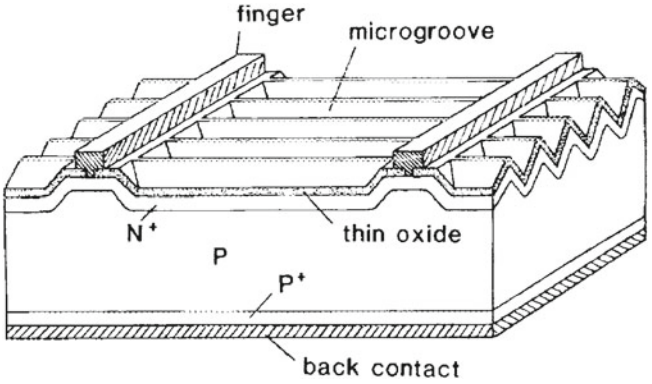

Fig. 2.13 The first 20 % efficient silicon solar cells present microgrooved surfaces [41]. The slats of 5 μm depth on a 10 μm pitch not only retain the refractive and anti-reflective advantages of pyramidally textured surfaces, but also avoid electrical transport resistances for lateral current flow to the collecting fingers. The finger metallization of the cell is further restricted to regions which have not been grooved

was textured with a 1D periodic slanted surface as apparent from Fig. 2.13, allowing both improved light-in coupling at oblique angles and a reduced electrical transport resistance.

The benefit of such anti-reflective v-shape textures were realized in the mid 70s [42] and also assisted in the demonstration of 14–17 % efficient but 400 μm thick silicon solar cells in 1977 [43].

I would describe the mid 80s as the foundation period for light-trapping in thin-film solar cells, when E. Yablonovitch and G. Cody highlighted the importance of random textures as a means to trap the light in the absorber slab [27]. The authors also explained how light-trapping allows to increase the optical absorption of a semiconductor by $4n^2$, if n is the index of refraction. Shortly thereafter, Sheng et al. [44] demonstrated that periodic textures can even exceed this limit in the weak absorption region, as discussed in Sect. 2.3.2.1.

Deckman et al. [45] were the first who experimentally demonstrated absorption enhancement factors of up to 12. The same authors also showed that the achievements were directly translated into 25 % higher short-circuit currents [46], though extremely thick a-Si:H absorber layers around 1 μm were used in both studies.

P. Campbell and M.A. Green then tried to determine the optical performance of pyramidal textures with respect to anti-reflection and light-trapping action [47]. The authors found the textures to yield high anti-reflection and refractive light-trapping, when the square based pyramids were at the front and a flat mirror at the back. The team later used such a texture to achieve a 24 % efficient silicon solar cell with 280 μm thickness [48].

The authors also recognized that the $4n^2$ limit would only be achieved if the previously mentioned 1D slanted surface texture in Fig. 2.13 was kept at the front and the same pattern applied to the rear side of the absorber, yet perpendicularly aligned with respect to the top one. For a silicon solar cell of about 100 μm thickness, such

an arrangement would outperform pyramidal structures on both sides by 4 % relative advantage in current generating according to their analysis [47].

At the end of the 80s, E. Yablonovitch provided further more background information and insights into the properties of a radiation field in a semiconductor [49]. Yablonovitch particularly focused on the consequences of artificially modifying the semiconductor with periodic structures. His paper about the "inhibited spontaneous emission in solid-state physics and electronics" is now recognized as one of the most important contributions to the field of photonics with more than 10,000 citations.

Contrary to intuition, he described light-trapping as the equivalence of restricting the spontaneous emission – which is the reversible process of photon absorption – into only those waveguide modes that are able to outcouple light from the material slab. The efficient operation of a solar cell does indeed require the re-emission of most absorbed photons back to the sun, because the electrical voltage increases with the re-emission rate. However, while the internal emission would be lost, the externally incident radiation becomes internally trapped, permitting the semiconductor slab to be correspondingly thinner – at the same degree of absorption. Yablonovitch thus interprets light-trapping and the reduction of semiconductor volume as a consequence of restricting the spontaneous emission into only the essential waveguide modes.

The 90s are then characterized by the expanding market of silicon solar cells. Germany and Japan are today seen as case studies for a government-driven PV market, because the two governments had initiated subsidy programs in order to spur adoption, e.g. they were the first to introduce feed-in tariffs (1990).

From the scientific perspective, the major focus was the development of new, large-scale and low-cost manufacturing techniques [50]. Chou et al. introduced the imprint lithography technique with 25 nm resolution [51], for example, whereas Gombert et al. [52] demonstrated moth-eye structures that were fabricateable on a large-scale. Two long-lasting record cells were also made at this time.

The first record was made by the Japanese company Kaneka [53]. They realized a device utilizing a natural **s**urface **t**exture for the **a**bsorption enhancement of a 2 μm thick polycrystalline silicon layer by a **r**ough back reflector (STAR). The STAR-cell was not only 100 times thinner than the first practical silicon solar cell had been [38], the 10.7 % efficiency was also almost twice as high as the original device and demonstrated that thin crystalline cells can achieve sufficient photon absorption by minute textured structures. The 90s may then also referred to as the decade of preparation for thin-film PV technology.

The second outstanding solar cell device was the PERL cell made by Zhao et al. [54] of Martin Green's group at UNSW, who were able to improve their former result by 2 % through reduced surface recombination losses. The use of a thin, thermally grown SiO_2 layer of about 20 nm thickness was found to effectively passivate the surface defects and allowed to establish the new performance level of 24.4 % efficiency in 1998. The device remained one of the top terrestrial silicon solar cells until 2013 [55]. Since the researchers were motivated by the fact that one third of the commercial PV products were based on large-grained multicrystalline silicon wafers (due to the lower costs), in the same mentioned study, the authors also showed a 6 % improvement in the efficiency of multicrystalline solar cells.

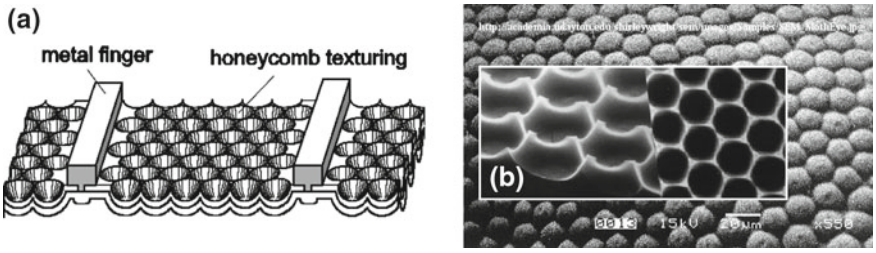

Fig. 2.14 **a** Schematic of a honeycomb surface texture for light-trapping. The texture could increase the optical path length of weakly absorbed light at 1060 nm wavelength by factors as high as 40 compared to a planar reference cell according to the authors [54]. However, such high enhancement factors are clearly not possible, because of the increased absorption in the rear metal reflector due to multiple light passes across the cell, which I will study later (Sect. 4.3) as one of the key issues of metals. **b** The SEM images show the perspective view (*left*) and a plan view (*right*) of a fabricated honeycomb surface structure on a large-grained polycrystalline silicon wafer. The spacing of the hexagons is 14 μm. Since the texture resembles a reversed moth-eye pattern, the background picture was inserted to highlight this similarity. The protuberances inside the combs – not present in the honeycomb texture – are responsible for the excellent anti-reflection properties

For multicrystalline silicon, anisotropic alkaline etching results in pyramids with completely random facets due to the uneven etch rates of the crystal planes [56]. The reflectance then becomes similar to an untextured surface according to J. Hylton [57]. The preferred texturing method for multicrystalline cells is therefore a wet isotropic acidic etching process [58].

Based on these observations, Zhao et al. [54] was able to texture the surface of a 260 μm thick multicrystalline wafer from Eurosolare with the honeycomb structure shown in Fig. 2.14, which enabled to obtain a 19.8 % power conversion efficiency. The authors showed that the refractive light-trapping properties of the hexagonal pattern were comparably effective to the inverted-pyramids used in monocrystalline silicon solar cells, but less efficient in terms of their anti-reflection action.

At the same time as M.A. Green published the intrinsic material function for crystalline silicon [59], Moharam [60], Whittaker [61] and co-authors outlined how the performance of light-trapping structures can be accurately simulated. These three papers provided the important groundwork for the emerging theoretical modelling period of diffractive light-trapping structures.

I see Shah's article in *Science* [62] both as the end of the long childhood of photovoltaics and as the begin of a thin-film silicon solar cell technology, because his review about the recent developments of photovoltaic solar modules concludes with the suggestion that thin-film crystalline silicon is becoming the prime candidate for future photovoltaics.

After the turn of the millenium, photovoltaics became a popular research subject, which is reflected by the number of publications in Fig. 2.15 and by the citation history of the paper from W. Shockley and H.J. Queisser [1]. According to W. Marx [2], the analysis by Shockley and Queisser has remained unnoticed for about 50 years, before the study literally attracted attention: the paper occupies the citation-rank number 12

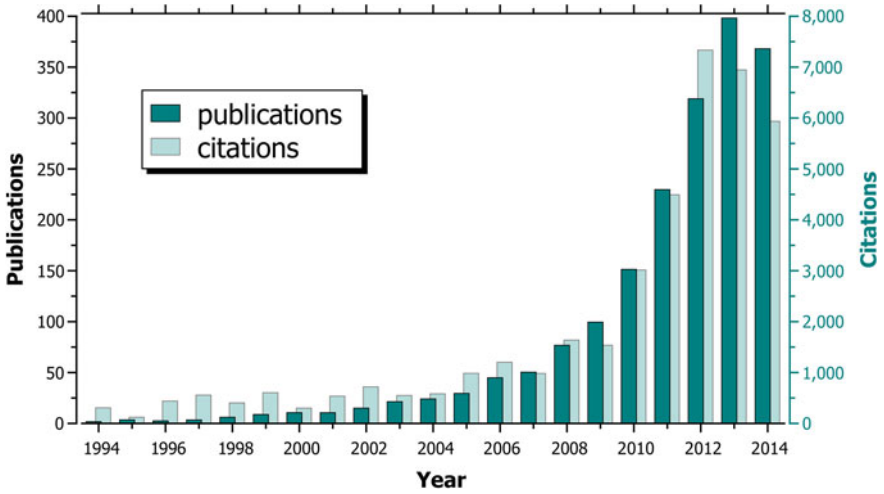

Fig. 2.15 Bibliographic analysis of publications (*left*) and citations (*right*) entered in the Web of Science (Thomson Reuters) before the 21st of November 2014. I used the keywords "light", "trapping" and "solar" and restricted the research areas to physics and optics. The total number of all publications is 2,000, whereas the number of all cited references is 38,000 in total. The exponential increase of research interest runs parallel with the steep increase of the cumulative PV capacity (not shown here). The silicon shortage between 2005 and 2008 could even have stimulated and intensified the scientific interest for light-trapping. For example, in 2005 a new article was published almost every week, while it ran up to one paper per day in 2012. Today, novel concepts, new strategies and emerging technologies in the PV field – like building-integrated, organic, dye-sensitized, plasmonic, CZTS, multi-junction, perovskite, HIT, flexible, hot-carrier, photon conversion, graphene, pentacene, quantum-dot or nanowire solar cells – make it easy to lose perspective

of all 11,723 physics papers entered in the Web of Science in 1961, and it attracted half of all citations from solar cell or photovoltaic papers for a 1961 paper [2].

2.5.2 The State of the Art

Light-trapping by random scattering (see Fig. 2.16) has since become the industrial standard for thin-film silicon modules [63]. At the same time, many novel methods for creating light scattering were introduced.

Metallic, dielectric 1D, 2D or 3D textures and photonic crystals were widely studied for their suitability for solar cells. The design optimization generally concentrated on the optical properties at the front (light in-coupling) or at the rear side (off-specular reflectance) of the thin-film absorber material. Structuring the back side normally addresses the red part of the spectrum only, since the blue and the green part of the visible spectrum are absorbed within the first few hundreds of nanometers in silicon. Therefore, patterning the absorber layer from both-sides increases

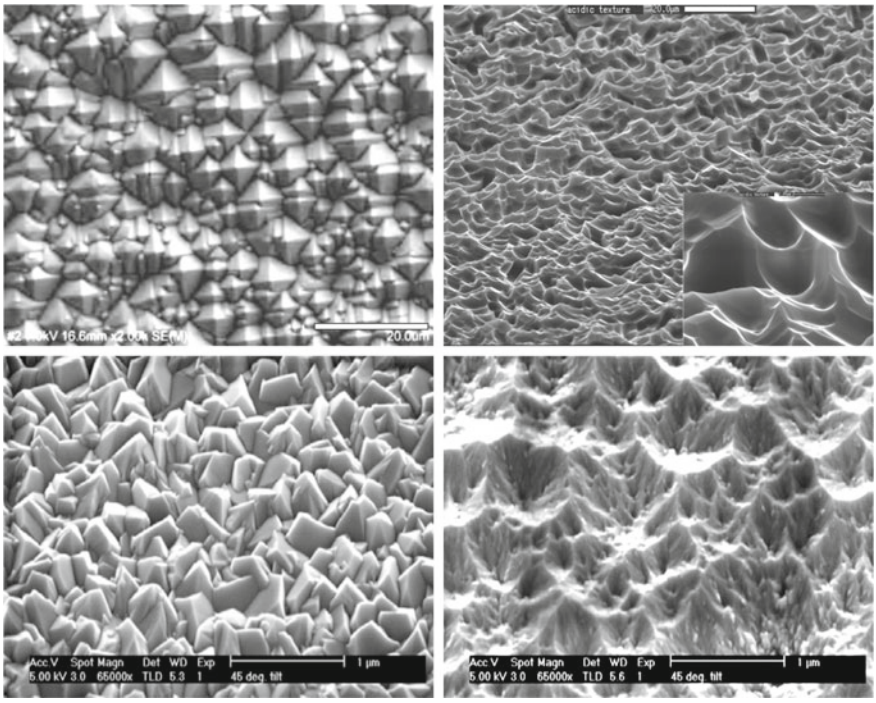

Fig. 2.16 Random surface textures increase the proportion of oblique scattered light into the absorber. Geometric light-trapping structures can easily be obtained in monocrystalline [67] (*top left*) or multicrystalline silicon [68] (*top right*) by chemical wet etching. Submicron light-trapping structures can form during the deposition, e.g. Asahi-U (*bottom left*), or may be chemically etched, e.g. into ZnO (*bottom right*) [69]

the degrees of freedom available to the designer, as anti-reflective (front side) and diffractive functions (back side) can be combined [64–66].

However, the advantages of using the strong scattering ability of *metallic* back reflectors are compromised by the substantial absorption losses in the metal itself. In the weak absorption limit, i.e. when light trapping is most beneficial, the light will interact even more often, so light-trapping, in fact, enhances parasitic absorption effects further. Campa et al. [70], for example, have found an overall reduction in the total reflectance of up to 40 % in comparison to a specular silver reflector.

Such optical losses may, in principle, be minimized when the metal is separated from the silicon by a transparent oxide layer [71], as obliquely incident light will likely be totally internally reflected at a silicon/dielectric interface. Conducting oxide spacer layers between the metal and silicon absorber material indeed became a standard in state-of-the-art light-trapping designs. Thin conductive oxides thus can play a significant role not only as transparent front electrode, but also in improving the back reflection properties [72]. Alternatively, the metal mirror at the back can be replaced with a distributed Bragg reflector [73, 74].

In order to identify the most promising light-trapping strategies, I applied the *LTE* defined in Eq. 2.25 to numerous structures found in the literature.

While the majority of proposals are numerical simulations based on (intrinsic) c-Si, experimental studies are often conducted on hydrogenated microcrystalline silicon (μ-Si:H) layers. Although the absorption coefficient of μ-Si:H depends on the defect density, crystalline/amorphous fraction and material morphology [75], its optical characteristic bears more similarity to c-Si than to a-Si:H. The *LTEs* of experimental structures for μ-Si:H absorber layers were thus qualitatively assessed with the optical constants of c-Si.

When the experimental reference was not provided for the total thickness, I decided to use the ideal short-circuit current as the unstructured reference in order to establish a minimum for the light trapping performance.

Unfortunately, designs based on amorphous silicon were excluded from the analysis, because of the large variations found in the optical material properties: the material absorption of hydrogenated amorphous silicon (a-Si:H) strongly depends on the hydrogen concentration and on deposition-conditions, and these were often not provided. For example, the optical band gap of a-Si:H substantially varies between 1.4 eV [76] and 2 eV [77]. Therefore, the literature analysis was applied to crystalline silicon (c-Si) where well-known optical properties are available [59].

Figure 2.17 summarizes the outcome of the assessed structures, while the corresponding short-circuit currents are listed in Tables 2.1, 2.2 and 2.3. For the assessment of the structures found in the literature, I applied the following four methods.

1. Absorption spectra. When only the numerical absorption spectra were shown [74], I used the free software tool Plot Digitizer from sourceforge.net and the standard global solar spectrum AM1.5G [78] in order to calculate the *LTE* of the structure.
2. Optical constants. As theoretical studies mainly use the optical constants provided by Green [59] or Palik [79], I tried to take this into account for the *LTE*. However, if J_{ref} appeared too close to the current of a single-pass traversal, I recalculated the reference with the same optical constants, e.g. [80].
3. Effective thickness. When authors compared their proposal to reference samples with the effective thickness, e.g. [47], I recalculated the short-circuit currents J_{MB} and J_{LL}, since in Eq. 2.25 all currents are defined for the same (total) absorber thickness. For the planar reference J_{ref}, I decided to use the ideal short-circuit current J_{MB} in order to establish a minimum for the light trapping performance.
4. Parasitic absorption. When authors compute the electrical current from absorption spectra, the charge-collection is generally assumed to be 100 %, i.e. every photogenerated charge-carrier contributes to the short-circuit current. Since the total absorption is decomposed into useful absorption in the silicon and parasitic absorption in other layers, the electrical current must refer to the sole active absorption only. I therefore excluded studies where I suspected parasitic influences. My criterion was a too high absorption near the wavelength bandgap of silicon.

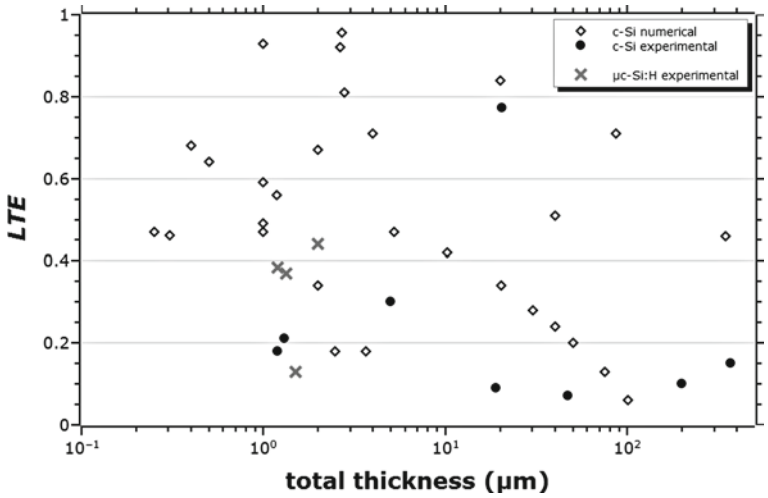

Fig. 2.17 The calculated light trapping efficiency *(LTE)* of light trapping structures realized or proposed in c-Si found in the literature (see Eq. 2.25). All µc-Si:H data points were assessed with the optical constants of c-Si [59]. While the *LTE* is, in principle, independent of the absorber thickness, the highest performing structures operate in the 1–5 µm range, which may relate to the fact that the benefit of light trapping is maximal in this thickness range. Notably, the solar cells with the highest efficiency (e.g. the 370 µm thick PERL cell) are not necessarily the best light trapping structures, highlighting the difference between the *LTE* and the absolute efficiency. This difference also highlights the importance of anti-reflection coatings, as already shown in Fig. 2.10

For a 300 µm thick silicon wafer, the absorption at 1100 nm wavelength will be greater than 7 % without back reflector and anti-reflection coating. For a 1 µm thin silicon slab with 100 % anti-reflection coating and lossless mirror, it requires a path length enhancement factor of $4n^2$ to absorb almost 2 % of the incident light, if $n = 3.54$ refers to the refractive index at 1100 nm wavelength. However, if the metal mirror were 99 % reflective, the parasitic loss may already sample to $1 - 0.99^{(2n^2)} > 20\,\%$, assuming the light is trapped by total internal reflection at the front and the metal mirror at the back.

The review allows me to conclude that light trapping is now close to being a solved problem, because several studies were able to achieve an *LTE* very close to the ideal 100 % performance. Naturally, demonstrating such high light-trapping efficiencies in real working solar cells still remains a challenging task.

As the key function of light-trapping structures is to enhance the absorption efficiency of a solar cell, it remains imperative to minimize the influence of the optical design on other process mechanisms that are involved in the conversion of the absorbed solar energy into electricity. So far, I could identify only one experimental structure approaching a $LTE \approx 80\,\%$, where nanotextures at the front and random pyramids at the back were designed in respect to high performance in anti-reflection and in light-trapping, respectively. The design also uses a silver mirror as back reflector, after a 100 nm SiO_2 was thermally grown on both sides of the structured 20 µm thick silicon absorber [72].

Table 2.1 The *LTE* of numerical structures using c-Si; only the best proposals in each reference were considered. The short-circuit currents are given in mA/cm^{-2}

LTE	Thickness (μm)	J_{max}	J_{ref}	J_{LL}	J_{MB}	References
0.96	2.7	33.9	23.2	36.2	25.0	[64]
0.93	1.0	29.1	15.0	33.5	18.3	[81]
0.92	2.7	35.7		36.6	25.0	[82]
0.84	20.0	37.3	31.3	41.1	34.0	[80]
0.81	2.8	34.6		36.8	25.3	[65]
0.71	4.0	32.0	24.8	37.6	27.6	[31]
0.71	86.7	42.0		43.3	38.8	[47]
0.68	0.4	21.8	10.3	29.6	12.5	[83]
0.67	2.0	29.4	21.0	35.7	23.0	[31]
0.64	0.5	21.5	12.0	28.7	13.8	[31]
0.59	1.0	25.4	16.5	33.3	18.3	[31]
0.56	1.2	27.6	19.4	34.1	19.4	[84]
0.51	40.0	36.4	33.7	42.3	37.0	[85]
0.47	5.2	33.6		38.4	29.2	[84]
0.47	0.3	16.4	8.3	27.2	9.9	[31]
0.47	1.0	24.2	17.1	33.5	18.3	[86]
0.46	0.3	20.1		30.2	11.4	[87]
0.46	346.7	43.0		44.5	41.7	[47]
0.42	10.2	35.7		39.9	32.6	[84]
0.34	2.0	23.6	19.3	35.8	23.1	[74]
0.34	20.3	37.2		41.2	35.2	[84]
0.28	30.2	37.9		41.9	36.3	[84]
0.24	40.2	38.3		42.3	37.1	[84]
0.20	50.2	38.6		42.7	37.6	[84]
0.18	2.5	26.7		36.5	24.5	[88]
0.18	3.7	29.0		37.5	27.1	[89]
0.13	75.3	39.1		43.2	38.5	[84]
0.06	100.3	39.4		43.5	39.2	[84]

2.6 Concluding Remarks

Analyzing the highest performing light-trapping structures [64, 65, 72, 80–82] allows to define three important design aspects: the control and modulation of the optical phase, the structuring of the absorber layer from both sides and the impact of surface textures on the electrical performance.

Table 2.2 The *LTE* of experimental structures using c-Si; only the best proposals in each reference were considered. The short-circuit currents are given in mA/cm^{-2}

LTE	Thickness (μm)	J_{max}	J_{ref}	J_{LL}	J_{MB}	References
0.77	20.5	39.3		40.6	34.8	[72]
0.30	5.0	17.5	14.7	38.3	29.0	[90]
0.21	1.3	15.5	12.5	34.4	20.1	[91]
0.19	1.5	15.4	12.8	34.8	20.9	[92]
0.15	370.0	40.9	40.5	44.5	41.8	[93]
0.10	200.0	41.0		44.1	40.6	[94]
0.09	19.0	35.5		41.1	35.0	[95]
0.07	47.0	37.8		42.6	37.4	[96]

Table 2.3 The *LTE* of experimental structures using μc-Si and qualitatively assessed with c-Si [59]; only the best proposals in each reference were considered. The short-circuit currents are given in mA/cm^{-2}

LTE	Thickness (μm)	J_{max}	J_{ref}	J_{LL}	J_{MB}	References
0.44	2.0	28.7		35.8	23.1	[97]
0.38	1.2	20.8	15.3	34.4	20.1	[18]
0.37	1.3	17.7	12.4	34.5	20.2	[98]
0.13	1.5	9.9	8.1	34.9	21.1	[90]

2.6.1 Phase Engineering

The benefit of a certain amount of disorder in periodic light-trapping structures was repeatedly confirmed in the past [31, 80, 99, 100], but some practical guidelines were given by Han and Chen [82], which were based on arguments of group theory as described in the following.

At first, the authors classify the waveguide modes into categories according to their symmetry properties under mirror reflection. Afterwards, they show that the mirror symmetries need to be broken to improve absorption, because the presence of mirror planes in a unit cell results in certain modes not coupling to incident light. The authors conclude that the symmetries can be broken either by destroying the periodic arrangements of the unit cell or by distorting the shape of the objects within the unit cell. They then argue that all modes will couple to light if the optical phase of any mode is not symmetric under mirror reflection.

Following the outlined strategy, the authors indeed achieve an $LTE = 0.92$ for 600 nm high skewed pyramids on a 2 μm thick c-Si absorber layer. Please note, that their method differs from breaking the symmetry of macroscopic structures where phase information is absent.

The conclusion, that a lack of structural symmetry improves the optical absorption, is also in agreement with results reported by other groups and for other geometries:

1. Peters et al. [101] compare and verify the similar light trapping properties of optimized periodic and stochastic structures having similar geometrical features. The choice of their texture was based on a particular pattern that had already been used to fabricate efficient thin-film silicon solar cells.
2. By the subtle superposition of multiple binary gratings, Martins and co-workers [81, 102] choose to tune the appropriate level of disorder into the unit cell via its Fourier spectrum. Their concept allowed the designers to obtain an $LTE = 0.93$ with a 190 nm etched QR code-like pattern on a 1 μm thick c-Si absorber. The design uses a 100 % reflective mirror on the back and a 70 nm nitride coating on the top to reduce avoidable reflection losses.
3. Ferry et al. [103] systematically study the relationship between photocurrent and the spatial correlations of random or designed surfaces. They evaluate four general classes of nanopatterns in terms of their Fourier transforms, which were obtained from AFM images, and used this as a basis for the calculation of the corresponding power spectral densities. The authors highlight that the essential design rule for strong photocurrent enhancements rests on the capability of tailoring the spatial frequencies in the structure to high scattering powers in the required range of optical frequencies.

Engineering light-trapping structures in terms of their impact on the optical phase thus can be understood as a general principle for enhancing the absorption of thin-films. Accordingly, whether a structure has a periodic or random morphology then tends to be less important than its *local* geometrical features, like the size and shape of the objects.

2.6.2 Dual Structuring

The benefit of structuring the absorber layer from both sides increases the degrees of freedom available to the designer, as different functions can be combined. For example, Wang et al. [65] suggested to optimize the front and back surface of a silicon slab for anti-reflection and light-trapping, respectively, due to the significant difference in the structural requirements. Their proposed dual-grating design uses circular nanocones as the basic building elements for the grating geometry on both the front and the back surfaces. However, its realization could turn out to be complicated by the detached back reflector configuration.

Structuring the absorber layer from both sides has often been proposed by many various authors [64–66, 104–108]. In fact, some of the best light-trapping structures listed in Tables 2.1, 2.2 and 2.3 actually adhere to this idea.

2.6.3 Electrical Performance

If an optically very good structure is electrically detrimental, or vice versa, the power conversion efficiency of a solar cell will be severely reduced.

1. From cross-sectional transmission electron microscopy (TEM) images Li et al. [109] show that the inability of conformal coverage tends to create pinholes in the cell, which are responsible for the electrical shunts. Using a textured substrate with a too high surface roughness for the deposition of the absorber material thus can result in short-circuiting of the entire device.
2. Sai et al. [97] are able to correlate the origin of carrier collection losses to the non-uniform coverage around concaves on the substrate surface. From SEM and TEM images they conclude that the period of a honeycomb lattice sets a threshold value for the maximum absorber thickness, which can be deposited onto the light-trapping structure free of cracks. Using a textured substrate with periodic structures and a too small period thus can result in electrical defects.
3. Texturing the silicon surface after the material deposition generally tends to increase the surface recombination velocity of charge carriers. However, Oh et al. [6] also measure higher Auger recombination rates in case the doping profile of the device was changed by the presence of the texture.
   Auger recombination is understood as the recombination of an electron-hole pair that is giving up its energy to an electron in the conduction band (instead to a photon). Since the extra kinetic energy of the Auger electron is given off to the silicon lattice, such lattice vibrations will likely increase the absorber temperature. Consequently, Auger recombinations are understood as heat loss, because solar energy is not converted into electricity.

Recently, Isabella et al. [64] tried to optimize the optical characteristics of a complete solar cell stack configuration by minimizing not only the parasitic absorption losses, but also the electrical losses. Their proposed light-trapping scheme uses a high aspect ratio texture at the front side for anti-reflective purposes and low aspect ratio random pyramids at the back side for efficient long-wavelength light scattering. The proposed design could theoretically ($LTE = 0.96$ [64]) and experimentally ($LTE = 0.77$ [72]) achieve the best light trapping efficiency.

References

1. W. Shockley, H.J. Queisser, Detailed balance limit of efficiency of p-n junction solar cells. AP **32**(3), 510–519 (1961). doi:10.1063/1.1736034
2. W. Marx, The shockley-queisser paper - a notable example of a scientific sleeping beauty. Ann. Phys. **526**(5–6), A41–A45 (2014). doi:10.1002/andp.201400806
3. H. Shen, Effect of c-si doping density on heterojunction with intrinsic thin layer (hit) radial junction solar cells, in *39th IEEE Photovoltaic Specialists Conference (PVSC)*, The Pennsylvania State University (2013), pp. 2466–2469. doi:10.1109/PVSC.2013.6744975

4. M. Gharghi, E. Fathi, B. Kante, S. Sivoththaman, X. Zhang, Heterojunction silicon microwire solar cells. Nano Lett. **12**(12), 6278–6282 (2012). doi:10.1021/nl3033813
5. Haoting Shen. Radial junction solar cells based on heterojunction with intrinsic thin layer (hit) structure. Dissertation, The Pennsylvania State University (2014), p. 167
6. J. Oh, H.-C. Yuan, H.M. Branz, An 18.2%-efficient black-silicon solar cell achieved through control of carrier recombination in nanostructures. Nature Nanotechnology **7**, 743–748 (2012). September. doi:10.1038/nnano.2012.166
7. X.X. Lin, X. Hua, Z.G. Huang, W.Z. Shen, Realization of high performance silicon nanowire based solar cells with large size. Nanotechnology **24**, 235402 (2013). doi:10.1088/0957-4484/24/23/235402
8. H.A. Atwater, A. Polman, Plasmonics for improved photovoltaic devices. Nat. Mater. **9**, 205–213 (2010). doi:10.1038/nmat2629
9. J. Park, J. Rao, T. Kim, S. Varlamov, Highest efficiency plasmonic polycrystalline silicon thin-film solar cells by optimization of plasmonic nanoparticle fabrication. Plasmonics **8**(2), 1209–1219 (2013). doi:10.1007/s11468-013-9534-x
10. V.E. Ferry, M.A. Verschuuren, H.B.T. Li, E. Verhagen, R.J. Walters, R.E.I. Schropp, H.A. Atwater, A. Polman, Light trapping in ultrathin plasmonic solar cells. Opt. Express **18**(S2), A237–A245 (2010). doi:10.1364/OE.18.00A237
11. H. Tan, R. Santbergen, A.H.M. Smets, M. Zeman, Plasmonic light trapping in thin-film silicon solar cells with improved self-assembled silver nanoparticles. Nano Lett. **12**, 4070–4076 (2012). doi:10.1021/nl301521z
12. H. Tan, L. Sivec, B. Yan, R. Santbergen, M. Zeman, A.H.M. Smets, Improved light trapping in microcrystalline silicon solar cells by plasmonic back reflector with broad angular scattering and low parasitic absorption. Appl. Phys. Lett. **102**, 153902 (2013). doi:10.1063/1.4802451
13. S. Morawiec, M.J. Mendes, S.A. Filonovich, T. Mateus, S. Mirabella, H. Águas, I. Ferreira, F. Simone, E. Fortunato, R. Martins, F. Priolo, I. Crupi, Broadband photocurrent enhancement in a-Si: H solar cells with plasmonic back reflectors. Opt. Express **22**(S4), A1059–A1070 (2014). doi:10.1364/OE.22.0A1059
14. P. Spinelli, M.A. Verschuuren, A. Polman, Broadband omnidirectional antireflection coating based on subwavelength surface mie resonators. Nat. Commun. **3**, 692 (2012). doi:10.1038/ncomms1691
15. J. Grandidier, D.M. Callahan, J.N. Munday, H.A. Atwater, Light absorption enhancement in thin-film solar cells using whispering gallery modes in dielectric nanospheres. Adv. Mater. **23**(10), 1272–1276 (2011). doi:10.1002/adma.201004393
16. E. Garnett, P. Yang, Light trapping in silicon nanowire solar cells. Nano Lett. **10**, 1082–1087 (2010). doi:10.1021/nl100161z
17. R. Santbergen, R. Liang, M. Zeman, a-si:h solar cells with embedded silver nanoparticles, in *35th IEEE Photovoltaic Specialists Conference (PVSC)* (2010), pp. 748–753. doi:10.1109/PVSC.2010.5617095
18. J. Müller, B. Rech, J. Springer, M. Vanecek, Tco and light trapping in silicon thin film solar cells. Sol. Energy **77**(6), 917–930 (2004). doi:10.1016/j.solener.2004.03.015
19. G.F. Zheng, J. Zhao, M. Gross, E. Chen, Very low light-reflection from the surface of incidence of a silicon solar cell. Sol. Energy Mater. Sol. Cells **40**(1), 89–95 (1996). doi:10.1016/0927-0248(95)00085-2
20. E. Jiménez-Rodríguez A. Montesdeoca-Santana, B. Gonzáilez-Díaz, D. Borchert, R. Guerrero-Lemus. Ultra-low concentration na_2co_3/$nahco_3$ solution for texturization of crystalline silicon solar cells. Prog. PV **20**(2), 191–196 (2012). doi:10.1002/pip.1117
21. S. Han, B.K. Paul, C. Chang, Nanostructured *ZnO* as biomimetic anti-reflective coatings on textured silicon using a continuous solution process. J. Mater. Chem. **22**(43), 22906–22912 (2012). doi:10.1039/C2JM33462C
22. B. Bläsi, Examples of photonic microstructures (2015). https://www.ise.fraunhofer.de/en/business-areas/solar-thermal-technology/research-topics/material-research-and-optics/fields-of-work/microstructured-surfaces/r-d-services/structure-examples
23. A. Fresnel, Mémoires sur la diffraction de la lumière. Oeuvres **1**, 89–122 (1816)

24. S. Larouche, D.R. Smith, Reconciliation of generalized refraction with diffraction theory. Opt. Lett. **37**(12), 2391–2393 (2012). doi:10.1364/OL.37.002391
25. C. Kittel, *Introduction to Solid State Physics* (Wiley, New York, 2004)
26. J.D. Joannopoulos, S.G. Johnson, J.N. Winn, R.D. Meade, *Photonic Crystals - Molding the Flow of Light* (Princeton University Press, Princeton, 2007)
27. E. Yablonovitch, G.D. Cody, Intensity enhancement in textured optical sheets for solar cells. IEEE Trans. Electron Devices **29**(2), 300–305 (1982). doi:10.1109/T-ED.1982.20700
28. J.H. Lambert, *Photometria, sive de mensura et gradibus luminis, colorum et umbrae* (W. Engelmann, Leipzig, 1892)
29. J. Gee, The effect of parasitic absorption losses on light trapping in thin silicon solar cells. IEEE PVSC Las Vegas **1**, 549–554 (1988). doi:10.1109/PVSC.1988.105762
30. C. Battaglia, M. Boccard, F.-J. Haug, C. Ballif, Light trapping in solar cells: when does a lambertian scatterer scatter lambertianly? Appl. Phys. **112**, 094504 (2012). doi:10.1063/1.4761988
31. A. Bozzola, M. Liscidini, L.C. Andreani, Photonic light-trapping versus lambertian limits in thin film silicon solar cells with 1D and 2D periodic patterns. Opt. Express **20**(S2), A224–A244 (2012). doi:10.1364/OE.20.00A224
32. Z. Yu, A. Raman, S. Fan, Fundamental limit of nanophotonic light trapping in solar cells. PNAS **107**(41), 17491–17496 (2010). doi:10.1073/pnas.1008296107
33. I.M. Peters, Phase space considerations for light path lengths in planar isotropic absorbers. Opt. Express Phase space considerations for light path lengths in planar, isotropic absorbers. **22**(S3), A908–A920 (2014). doi:10.1364/OE.22.00A908
34. A. Basch, F.J. Beck, T. Söderström, S. Varlamov, K.R. Catchpole, Combined plasmonic and dielectric rear reflectors for enhanced photocurrent in solar cells. APL **100**, 243903 (2012). doi:10.1063/1.4729290
35. F. Pratesi, M. Burresi, F. Riboli, K. Vynck, D.S. Wiersma, Disordered photonic structures for light harvesting in solar cells. Opt. Express **21**(S3), A460–A468 (2013). doi:10.1364/OE.21.00A460
36. R.S. Ohl, Light-sensitive electric device (1946). http://www.google.com/patents/US2402662 (US Patent 2402662)
37. I.M. Ross, The invention of the transistor. IEEE **86**(1), 7–28 (1998). doi:10.1109/5.658752
38. D.M. Chapin, C.S. Fuller, G.L. Pearson, A new silicon p–n junction photocell for converting solar radiation into electrical power. AP **25**, 676/677 (1954). doi:10.1063/1.1721711
39. G.K. Teal, Some recent developments in silicon and germanium materials and devices, in *National Conference on Airborne Electronics Dayton (Ohio)* (1954)
40. G.K. Teal, J.B. Little, Growth of germanium single crystals. Phys. Rev. **78**, 647 (1950). doi:10.1103/PhysRev.78.637
41. A.W. Blakers, M.A. Green, 20% efficiency silicon solar cells. APL **48**(3), 215–217 (1986). doi:10.1063/1.96799
42. C.R. Baraona, H.W. Brandhorst, V-grooved silicon solar cells, in *IEEE 11th Photovoltaic Specialists Conference in Phoenix (Arizona)* (1975)
43. M.S. Bae, R.V. O'Aielio, p+/n high-efficiency silicon solar cells. APL **31**, 285 (1977). doi:10.1063/1.89664
44. P. Sheng, A.N. Bloch, R.S. Stepleman, Wavelength-selective absorption enhancement in thin-film solar cells. Appl. Phys. Lett. **43**(6), 579–581 (1983). doi:10.1063/1.94432
45. H.W. Deckman, C.B. Roxlo, E. Yablonovitch, Maximum statistical increase of optical absorption in textured semiconductor films. Opt. Lett. **8**(9), 491–493 (1983a). doi:10.1364/OL.8.000491
46. H.W. Deckman, C.R. Wronski, H. Witzke, E. Yablonovitch, Optically enhanced amorphous silicon solar cells. APL **42**(11), 968–970 (1983b). doi:10.1063/1.93817
47. P. Campbell, M.A. Green, Light trapping properties of pyramidally textured surfaces. AP **62**, 243 (1987). doi:10.1063/1.339189
48. J. Zhao, A. Wang, M.A. Green, 24% efficient perl structure silicon solar cells. IEEE Photovolt. Spec. Conf. (Kissimmee) **1**, 333–335 (1990). doi:10.1109/PVSC.1990.111642

49. E. Yablonovitch, Inhibited spontaneous emission in solid-state physics and electronics. Phys. Rev. Lett. **58**(20), 2059–2062 (1987). doi:10.1103/PhysRevLett.58.2059
50. J. Szlufcik, S. Sivoththaman, J.F. Nijs, R.P. Mertens, R. van Overstraeten, Low-cost industrial technologies of crystalline silicon solar cells. IEEE **85**(5), 711–730 (1997). doi:10.1109/5.588971
51. S. Chou, P. Krauss, P. Renstrom, Imprint lithography with 25-nanometer resolution. Science **272**(5258), 85–87 (1996). doi:10.1126/science.272.5258.85
52. A. Gombert, K. Rose, A. Heinzel, W. Horbelt, C. Zanke, B. Bläsi, W. Wittwer, Antireflective submicrometer surface-relief gratings for solar applications. SEM **54**, 333–342 (1998). doi:10.1016/S0927-0248(98)00084-1
53. K. Yamamoto, M. Yoshimi, T. Suzuki, Y. Tawada, Y. Okamoto, A. Nakajima, Thin film poly-si solar cell on glass substrate fabricated at low temperature. MRS Spring Meeting on Amorphous and Microcrystalline Silicon Technology (San Francisco) **507**, 131–138 (1998)
54. J. Zhao, A. Wang, M.A. Green, F. Ferrazza, 19.8% efficient "honeycomb" textured multicrystalline and 24.4 % monocrystalline silicon solar cells. APL **73**(14), 1991–1993 (1998). doi:10.1063/1.122345
55. M.A. Green, K. Emery, Y. Hishikawa, W. Warta, E.D. Dunlop, Solar cell efficiency tables (version 43). Prog. PV: Res. Appl. **22**, 1–9 (2014). doi:10.1002/pip.2452
56. R. Sinton, Y. Kwark, J. Gan, R. Swanson, 27.5-percent silicon concentrator solar cells. IEEE Electron Device Lett. **7**(10), 567–569 (1986). doi:10.1109/EDL.1986.26476
57. J. Hylton, Light coupling and light trapping in alkaline etched multicrystalline silicon wafers for solar cells. Ph.D. thesis, University of Utrecht (2006)
58. R. Einhaus, E. Vazsonyi, J. Szlufcik, J. Nijs, R. Mertens, Isotropic texturing of multicrystalline silicon wafers with acidic texturing solutions, in *IEEE Photovoltaic Specialists Conference Anaheim (CA)* (1997), pp. 167–170. doi:10.1109/PVSC.1997.654055
59. M.A. Green, M.J. Keevers, Short communication: optical properties of intrinsic silicon at 300 k. Prog. PV: Res. Appl. **3**, 189–192 (1995). doi:10.1002/pip.4670030303
60. M.G. Moharam, E.B. Grann, D.A. Pommet, Formulation for stable and efficient implementation of the rigorous coupled-wave analysis of binary gratings. J. OSA **12**(5), 1068–1076 (1995). doi:10.1364/JOSAA.12.001068
61. D.M. Whittaker, I.S. Culshaw, Scattering-matrix treatment of patterned multilayer photonic structures. PRB **60**, 2610 (1999). doi:10.1103/PhysRevB.60.2610
62. A. Shah, P. Torres, R. Tscharner, N. Wyrsch, H. Keppner, Photovoltaic technology: the case for thin-film solar cells. Science **285**(5428), 692–698 (1999). doi:10.1126/science.285.5428.692
63. C. Battaglia, C.-M. Hsu, K. Söderström, J. Escarré, F.-J. Haug, M. Charrière, M. Boccard, M. Despeisse, D.T.L. Alexander, M. Cantoni, Y. Cui, C. Ballif, Light trapping in solar cells: can periodic beat random? ACS Nano **6**(3), 2790–2792 (2012b). doi:10.1021/nn300287j
64. O. Isabella, A. Ingenito, D. Linssen, M. Zeman, Front/rear decoupled texturing in refractive and diffractive regimes for ultra-thin silicon-based solar cells, in *Renewable Energy and the Environment, OSA Technical Digest* (2013), p. PM4C.2. doi:10.1364/PV.2013.PM4C.2
65. K.X. Wang, Z. Yu, V. Liu, Y. Cui, S. Fan, Absorption enhancement in ultrathin crystalline silicon solar cells with antireflection and light-trapping nanocone gratings. Nano Lett. **12**(3), 1616–1619 (2012). doi:10.1021/nl204550q
66. C.S. Schuster, P. Kowalczewski, E.R. Martins, M. Patrini, M.G. Scullion, M. Liscidini, L. Lewis, C. Reardon, L.C. Andreani, T.F. Krauss, Dual gratings for enhanced light trapping in thin-film solar cells by a layer-transfer technique. Opt. Express **21**(S3), A433–A439 (2013). doi:10.1364/OE.21.00A433
67. J. Gjessing, Photonic crystals for light trapping in solar cells. Ph.D. thesis, University of Oslo (2011)
68. D. Macdonald, A. Cuevas, M. Kerr, C. Samundsett, D. Ruby, S. Winderbaum, A. Leo, Texturing industrial multicrystalline silicon solar cells. Sol. Energy **76**, 277–283 (2004). doi:10.1016/j.solener.2003.08.019

69. O. Isabella, K. Jäger, J. Krc, M. Zeman, Light scattering properties of surface-textured substrates for thin-film solar cells. Proc. 23rd EUPVSEC **1**, 476–481 (2008)
70. A. Čampa, J. Krč, F. Smole, M. Topič, Potential of diffraction gratings for implementation as a metal back reflector in thin-film silicon solar cells. TSF **516**(20), 6963–6967 (2008). doi:10.1016/j.tsf.2007.12.051
71. H. Sai, H. Fujiwara, M. Kondo, Back surface reflectors with periodic textures fabricated by self-ordering process for light trapping in thin-film microcrystalline silicon solar cells. SEM **93**, 1087–1090 (2009). doi:10.1016/j.solmat.2008.12.030
72. A. Ingenito, O. Isabella, M. Zeman, Experimental demonstration of $4n2$ classical absorption limit in nanotextured ultrathin solar cells with dielectric omnidirectional back reflector. ACS Photonics **1**(3), 270–278 (2014). doi:10.1021/ph4001586
73. L. Zeng, Y. Yi, C. Hong, J. Liu, N. Feng, X. Duan, L.C. Kimerling, B.A. Alamariu, Efficiency enhancement in si solar cells by textured photonic crystal back reflector. APL **89**, 11 (2006). doi:10.1063/1.2349845
74. P. Bermel, C. Luo, L. Zeng, L.C. Kimerling, J.D. Joannopoulos, Improving thin-film crystalline silicon solar cell efficiencies with photonic crystals. OE **15**(25), 16986–17000 (2007). doi:10.1364/OE.15.016986
75. A. Poruba, A. Fejfar, Z. Remes, J. Springer, M. Vanecek, J. Kocka, J. Meier, P. Torres, A. Shah, Optical absorption and light scattering in microcrystalline silicon thin films and solar cells. AP **88**(1), 148–160 (2000). doi:10.1063/1.373635
76. G.D. Cody, T. Tiedje, B. Abeles, B. Brooks, Y. Goldstein, Disorder and the optical-absorption edge of hydrogenated amorphous silicon. Phys. Rev. Lett. **47**(20), 1480 (1981). doi:10.1103/PhysRevLett.47.1480
77. N. Bakr, A. Funde, V. Waman, M. Kamble, R. Hawaldar, D. Amalnerkar, S. Gosav, S. Jadkar, Determination of the optical parameters of a-si:h thin films deposited by hot wire-chemical vapour deposition technique using transmission spectrum only. Pramana **76**(3), 519–531 (2011). doi:10.1007/s12043-011-0024-4
78. Am1.5g solar spectrum irradiance data, 2015. http://rredc.nrel.gov/solar/spectra/am1.5
79. E.D. Palik, *Handbook of Optical Constants of Solids* (Academic, Orlando, 1985)
80. J. Gjessing, A.S. Sudbø, E.S. Marstein, Comparison of periodic light-trapping structures in thin crystalline silicon solar cells. J. Appl. Phys. **110**(3), 033104 (2011). doi:10.1063/1.3611425
81. E.R. Martins, J. Li, Y. Liu, V. Depauw, Z. Chen, J. Zhou, T.F. Krauss, Deterministic quasi-random nanostructures for photon control. Nat. Commun. **4**, 2665 (2013). doi:10.1038/ncomms3665
82. S.E. Han, G. Chen, Toward the lambertian limit of light trapping in thin nanostructured silicon solar cells. Nano Lett. **10**(11), 4692–4696 (2010). doi:10.1021/nl1029804
83. S.B. Mallick, M. Agrawal, P. Peumans, Optimal light trapping in ultra-thin photonic crystal crystalline silicon solar cells. Opt. Express **18**(6), 5691–5706 (2010). doi:10.1364/OE.18.005691
84. A. Mellor, I. Tobias, A. Marti, A. Luque, A numerical study of bi-periodic binary diffraction gratings for solar cell applications. Sol. Energy Mater. Sol. Cells **95**(12), 3527–3535 (2011). doi:10.1016/j.solmat.2011.08.017
85. A. Mellor, H. Hauser, C. Wellens, J. Benick, J. Eisenlohr, M. Peters, A. Guttowski, I. Tobías, A. Martí, A. Luque, B. Bläsi, Nanoimprinted diffraction gratings for crystalline silicon solar cells: implementation, characterization and simulation. Opt. Express **21**(S2), A295–A304 (2013). doi:10.1364/OE.21.00A295
86. R. Dewan, D. Knipp, Light trapping in thin-film silicon solar cells with integrated diffraction grating. J. Appl. Phys. **106**(7), 074901 (2009). doi:10.1063/1.3232236
87. Y. Yao, J. Yao, V. Kris Narasimhan, Z. Ruan, C. Xie, S. Fan, Y. Cui, Broadband light management using low-q whispering gallery modes in spherical nanoshells. Nat. Commun. **3**, 664 (2012). doi:10.1038/ncomms1664
88. N.T. Fofang, T.S. Luk, M. Okandan, G.N. Nielson, I. Brener, Substrate-modified scattering properties of silicon nanostructures for solar energy applications. Opt. Express **21**(4), 4774–4782 (2013). doi:10.1364/OE.21.004774

89. D. Lockau, T. Sontheimer, C. Becker, E. Rudigier-Voigt, F. Schmidt, B. Rech, Nanophotonic light trapping in 3-dimensional thin-film silicon architectures. Opt. Express **21**(S1), A42–A52 (2013). doi:10.1364/OE.21.000A42
90. X. Sheng, L.Z. Broderick, L.C. Kimerling, Photonic crystal structures for light trapping in thin-film si solar cells: modeling, process and optimizations. Opt. Commun. **314**, 41–47 (2014). doi:10.1016/j.optcom.2013.07.085
91. C. Trompoukis, O. El Daif, V. Depauw, I. Gordon, J. Poortmans, Photonic assisted light trapping integrated in ultrathin crystalline silicon solar cells by nanoimprint lithography. Appl. Phys. Lett. **101**(10), 103901 (2012). doi:10.1063/1.4749810
92. V. Depauw, X. Meng, O. El Daif, G. Gomard, L. Lalouat, E. Drouard, C. Trompoukis, A. Fave, C. Seassal, I. Gordon, Micrometer-thin crystalline-silicon solar cells integrating numerically optimized 2-d photonic crystals. IEEE J. Photovolt. **4**(1), 215–223 (2013). doi:10.1109/JPHOTOV.2013.2286521
93. J. Zhao, A. Wang, P.P. Altermatt, S.R. Wenham, M.A. Green, 24% efficient perl silicon solar cell: recent improvements in high efficiency silicon cell research. Sol. Energy Mater. Sol. Cells **41**(42), 87–99 (1996). doi:10.1016/0927-0248(95)00117-4
94. F. Feldmann, M. Bivour, C. Reichel, M. Hermle, S.W. Glunz, A passivated rear contact for high-efficiency n-type si solar cells enabling high voc's and *ff* > 82%, in *28th EU PVSEC* (2013), p. 2CO.4.4. doi:10.4229/28thEUPVSEC2013-2CO.4.4
95. L. Wang, J. Han, A. Lochtefeld, A. Gerger, M. Carroll, D. Stryker, S. Bengtson, M. Curtin, H. Li, Y. Yao, D. Lin, J. Ji, A.J. Lennon, R.L. Opila, A. Barnett, 16.8% efficient ultrathin silicon solar cells on steel, in *28th EU PVSEC* (2013), p. 3DV.1.12. doi:10.4229/28thEUPVSEC2013-3DV.1.12
96. J.H. Petermann, D. Zielke, J. Schmidt, F. Haase, E.G. Rojas, R. Brendel, 19% efficient and 43 μm thick crystalline si solar cell from layer transfer using porous silicon. Prog. Photovolt. Res. Appl. **20**(1), 1–5 (2012). doi:10.1002/pip.1129
97. H. Sai, K. Saito, N. Hozuki, M. Kondo, Relationship between the cell thickness and the optimum period of textured back reflectors in thin-film microcrystalline silicon solar cells. Appl. Phys. Lett. **102**, 053509 (2013). doi:10.1063/1.4790642
98. C. Haase, H. Stiebig, Optical properties of thin-film silicon solar cells with grating couplers. Prog. Photovolt. Res. Appl. **14**(7), 629–641 (2006). doi:10.1002/pip.694
99. C. Heine, R. Morf, Submicrometer gratings for solar energy applications. Appl. Opt. **34**(14), 2476–2482 (1995). doi:10.1364/AO.34.002476
100. A. Lin, J. Phillips, Optimization of random diffraction gratings in thin-film solar cells using genetic algorithms. SEM **92**, 1689–1696 (2008). doi:10.1016/j.solmat.2008.07.021
101. M. Peters, C. Battaglia, K. Forberich, B. Bläsi, N. Sahraei, A.G. Aberle, Comparison between periodic and stochastic parabolic light trapping structures for thin-film microcrystalline silicon solar cells. Opt. Express **20**(28), 29488–29499 (2012). doi:10.1364/OE.20.029488
102. E.R. Martins, J. Li, Y.K. Liu, J. Zhou, T.F. Krauss, Engineering gratings for light trapping in photovoltaics: The supercell concept. Phys. Rev. B **86**, 041404(R) (2012). doi:10.1103/PhysRevB.86.041404
103. V.E. Ferry, M.A. Verschuuren, M. Claire van Lare, R.E.I. Schropp, H.A. Atwater, A. Polman, Optimized spatial correlations for broadband light trapping nanopatterns in high efficiency ultrathin film a-si:h solar cells. Nano Lett. **11**, 4239–4245 (2011). doi:10.1021/nl202226r
104. R. Dewan, M. Marinkovic, R. Noriega, S. Phadke, A. Salleo, D. Knipp, Light trapping in thin-film silicon solar cells with submicron surface texture. Opt. Express **17**(25), 23058–23065 (2009). doi:10.1364/OE.17.023058
105. D. Madzharov, R. Dewan, D. Knipp, Influence of front and back grating on light trapping in microcrystalline thin-film silicon solar cells. Opt. Express **19**(S2), A95–A107 (2011). doi:10.1364/OE.19.000A95
106. M.A. Tsai, H.W. Han, Y.L. Tsai, P.C. Tseng, P. Yu, H.C. Kuo, C.H. Shen, J.M. Shieh, S.H. Lin, Embedded biomimetic nanostructures for enhanced optical absorption in thin-film solar cells. Opt. Express **19**(S4), A757–A762 (2011). doi:10.1364/OE.19.00A757

107. A. Abass, K.Q. Le, A. Alù, M. Burgelman, B. Maes, Dual-interface gratings for broadband absorption enhancement in thin-film solar cells. Phys. Rev. B **85**(11), 115449 (2012). doi:10.1103/PhysRevB.85.115449
108. X. Meng, E. Drouard, G. Gomard, R. Peretti, A. Fave, C. Seassal, Combined front and back diffraction gratings for broad band light trapping in thin film solar cell. Opt. Express **20**(S5), A560–A571 (2012). doi:10.1364/OE.20.00A560
109. H.B.T. Li, R.H.-J. Franken, R.L. Stolk, J.K. Rath, R.E.I. Schropp, Mechanism of shunting of nanocrystalline silicon solar cells deposited on rough Ag/ZnO substrates. Solid State Phenom. **131–133**, 27–32 (2007). doi:10.4028/www.scientific.net/SSP.131-133.27

http://www.springer.com/978-3-319-44277-8

Diffractive Optics for Thin-Film Silicon Solar Cells

Schuster, C.S.

2017, XX, 114 p. 56 illus., 11 illus. in color., Hardcover
ISBN: 978-3-319-44277-8